Interface crack onset at a circular cylindrical inclusion under a remote transverse tension. Application of a coupled stress and energy criterion

V. Mantič[1]

Group of Elasticity and Strength of Materials, School of Engineering
University of Seville, Camino de los Descubrimientos s/n, 41092 Seville, Spain

November 4, 2008

Abstract

The plane strain problem of a single circular cylindrical inclusion embedded in an unbounded matrix subjected to a remote uniform uniaxial transverse tension is studied. A theoretical model for the simultaneous prediction of *the initial size of a crack originated at the inclusion/matrix interface* (or equivalently the initial polar angle of this crack) and of *the critical remote tension required to originate this crack* is developed. Isotropic and linear elastic behaviour of both materials, with the inclusion being stiffer than the matrix, is assumed. The interface is considered to be strong (providing continuity of displacements and tractions across the interface surface) and brittle. The model developed is based on the classical analytic solutions for the above-mentioned inclusion problem without and with a crack situated at the inclusion/matrix interface and a recently introduced coupled stress and energy criterion of failure by Leguillon (*Eur. J. Mech. A/Solids, 21, pp. 61–72, 2002*). A new dimensionless structural parameter γ, depending on bimaterial and interface properties together with the inclusion radius a, which plays a key role in characterizing the interface crack onset, is introduced. Asymptotic behaviour of the predicted critical remote tension and the interface crack length/polar angle at the onset are characterized for small and large values of γ and a. A size effect inherent to this problem is predicted and analysed. The following asymptotic characteristics of this size effect are noteworthy: *i)* for small inclusion radii a, the polar angle of the crack at onset is constant (independent of a), whereas the critical remote tension increases with decreasing a, being inversely proportional to the square root of a; *ii)* for large inclusion radii a, the length of the crack at onset and the critical remote tension are approximately constant.

Keywords: inclusion debond, interface crack, crack nucleation, strength, fracture toughness, finite fracture mechanics, size effect, scaling, brittleness number, composites.

1 Introduction

It is well known that stiff circular cylindrical inclusions embedded in a compliant matrix subjected to a remote transverse tension act as stress concentrators of radial and shear stresses, σ_r and $\sigma_{r\theta}$ (referring to a polar coordinate system centered at each inclusion), at the inclusion/matrix interfaces. The most representative industrial application of this inclusion/matrix system are Fibre Reinforced Composites (FRC). The failure mechanism in FRC under traverse tension loads, called 'matrix cracking' or 'interfibre failure', typically initiates as partial debonds at fibre/matrix interfaces (or as matrix voids near this interface) due to the above-mentioned stress concentrations therein. These debonds (voids) grow as cracks along (close to) the fibre/matrix interface, eventually, under certain conditions, leaving the interface and penetrating into the matrix, where the coalescence of these cracks originates macrocracks in the composite. Any improvement in the capability of predicting the development of these cracks in FRC would be of great importance for the design and evaluation of composite structures.

The above-described failure mechanism, one of the common modes of failure of FRC, has been studied from the micromechanical point of view, considering a single fibre embedded in a matrix, in many previous theoretical, numerical and experimental works, see for instance England (1966); Toya (1974); París et al. (1996); Chao (1997); Varna et al. (1997a,b); Zhang et al. (1997); Prasad (2003); París et al. (2007). Nevertheless, the question of the partial debond initiation at the originally undamaged fibre/matrix interface has still not been addressed in a satisfactory manner, to the best knowledge of the author.

In general, either a stress based criterion or an energy based criterion is used to analyse a failure initiation and its further growth. Nevertheless, the crack onset at the (originally undamaged) inclusion/matrix interface

[1] On leave at the Computer Science and Mathematics Division, Oak Ridge National Laboratory, Oak Ridge, TN 37831, U.S.A.

cannot be correctly predicted by an individual application of either of these two criteria. Each one has its own difficulties, when used in the present problem, to predict the critical remote load originating a partial debond at the originally undamaged inclusion/matrix interface.

The normal stress criterion predicts rupture at those interface points where the local value of the normal traction is greater than the tensile strength of the interface. Hence, due to the non constant distribution of the normal tractions along the undamaged inclusion/matrix interface (known from works by Goodier (1933); Hardiman (1954); Honein and Herrmann (1990)), the predicted polar angle of the crack at onset depends on the predicted critical value of the remote load and viceversa. Thus, the dilemma of this criterion lies in the fact that it provides only one equation for two unknowns.

The energy criterion, in the framework of classical Fracture Mechanics, compares the Energy Release Rate (ERR) evaluated for a hypothetical infinitesimal crack at the inclusion/matrix interface with a finite value of the interface fracture toughness. However, a consequence of the fact that no stress singularity is present at the originally undamaged interface is that this ERR vanishes for an infinitesimally small crack (see Toya (1974)). This paradoxically implies that an infinitesimal crack nucleation is not possible according to this criterion.

To solve difficulties of this kind Leguillon (2002) proposed a coherent approach combining both criteria in the framework of Finite Fracture Mechanics (for a review see Taylor et al. (2005)), which, as opposed to the usual Fracture Mechanics models, does not need an initial crack length to work properly. Two necessary conditions, given by a pointwise stress criterion and an incremental global energy criterion, for an abrupt formation of a crack of a finite extension, are established in this approach. In this way both above-described difficulties of the individually applied criteria are solved, providing two equations for two unknowns, the critical load and the finite crack length at onset.

Although similar approaches based on coupling stress and energy criteria to predict fracture or void nucleation have been known for a relatively long time, e.g. Fisher and Gurland (1981) (see also Tszeng (1993) for a review), it seems that only the recent Leguillon's (2002) proposal has been widely accepted, and several new successful applications of this approach to fracture onset in problems with singularities and stress concentrations have appeared in recent years, see e.g. Leguillon and Siruguet (2002); Cornetti et al. (2006); Leguillon et al. (2007); Carpinteri et al. (2008). Nevertheless, to the author's best knowledge, the full potential of this coupled stress and energy criterion to characterize the fracture onset at the inclusion/matrix interface, and particularly in the present case of circular cylindrical inclusion, has still not been fully explored.

Moreover, Leguillon et al. (2007) have shown that this coupled stress and energy criterion can explain a size effect for blunt notches and cavities. With reference to composites, the effect of inclusion size on their mechanical performance has been addressed by many authors (see e.g. Leidner and Woodhams (1974); Fisher and Gurland (1981); Cho et al. (2006)), demonstrating that, in general, the tensile strength of composites increases as the size of inclusions decreases, which is associated to the fact that a higher level of load is required to nucleate cracks at smaller inclusions than at larger ones. The interest in this inclusion size effect has recently been revived with the appearance of nanocomposites, where higher failure loads are expected in comparison with traditional composites. Thus, an analysis of the expected size effect predictions by the coupled stress and energy criterion can significantly contribute to understanding composite strength.

The purpose of the present work is to contribute to modeling the abrupt formation of an inclusion/matrix debond in FRC. In particular, it aims to provide a new look (based on the coupled stress and energy criterion) at the debond onset at a circular cylindrical inclusion embedded in a matrix subjected to a remote uniaxial transverse tension. The crack onset is assumed to happen in a symmetric situation with respect to the load direction and at one side of the inclusion only. This appears to be a frequently observed configuration in real unidirectional plies subjected to a sufficiently large transverse tension load (see experimental results shown in Zhang et al. (1997); París et al. (2007)). Recall that a further debond growth as an interface crack, not studied here, can be analysed in a similar way to that carried out by París et al. (2007).

In the present work, isotropic and linear elastic behaviour of both materials, with the inclusion being stiffer than the matrix, is assumed. The inclusion/matrix interface is considered to be strong (providing continuity of displacements and tractions across the interface surface) and brittle. The interface is characterized by its tensile strength and fracture toughness curve. The debond onset at this interface is assumed to have the form of a sharp crack. Hence, the present inclusion/matrix debonding is treated in the framework of Interface Fracture Mechanics. Two basic models have been developed in the past for the analysis of interface cracks: the open model, which assumes traction free crack faces, Williams (1959), and the contact model, which assumes a contact zone adjacent to each crack tip, Comninou (1977). For a comprehensive review of these models, in particular of their relations and limitations, see Rice (1988); Hutchinson and Suo (1992); Hills and Barber (1993); Hills et al. (1996); Gerberich and Yang (2003); Mantič et al. (2006). With reference to the present problem of the interface crack onset, hence considering relatively small debond angles, for instance semidebond

angles below 60°, the open model is considered appropriate for the required fracture assessment. This is due to the very small zone of non-compatible interpenetrations adjacent to the crack tip (inherent to the open model) for such semidebond angles, as follows from the analysis performed by several authors, e.g. Toya (1974); París et al. (1996); Chao (1997); Varna et al. (1997a). Nevertheless, a study of the further debond growth (not intended in the present work), corresponding to greater semidebond angles, may require the application of the contact model as well, cf. París et al. (2007).

The procedure developed in the present work, applying the approach introduced by Leguillon (2002) to the present problem, uses several solutions, enumerated below, which are available in closed analytic form in the literature:

(i) The analytic solution for stresses along the undamaged inclusion/matrix interface (Goodier (1933); Hardiman (1954); Honein and Herrmann (1990)), to be applied in the stress criterion.

(ii) The analytic solution of the open model for stresses ahead of a crack at the inclusion/matrix interface (England (1966); Toya (1974)), to be applied for the evaluation of the fracture mode mixity of the interface crack in the energy criterion.

(iii) The ERR in the open model for a crack at the inclusion/matrix interface (Toya (1974)), to be used in the energy criterion.

(iv) A phenomenological law estimating the fracture toughness curve—the variation of the interface fracture toughness as a function of the fracture mode mixity of an interface crack (Hutchinson and Suo (1992)), to be used in the energy criterion.

It has been useful for the purposes of the present work to rewrite the solutions in *i)–iii)* in terms of the Dundurs (1969) bimaterial parameters α and β, which in addition to an easy parametric study has allowed some interesting and useful relationships between these solutions to be elucidated.

After a short review of the elastic bimaterial constants in Section 2, the stress solution along the undamaged interface *(i)* is presented and studied in Section 3. The stress solution ahead of an interface crack *(ii)* and the associated ERR *(iii)* are shown and analysed in Section 4. Although the present work is focused on the stiff inclusion embedded in a compliant matrix ($\alpha, \beta > 0$), the results shown in Sections 3 and 4 cover in fact the whole range of isotropic bimaterials. The coupled stress and energy criterion is applied to the present problem in Section 5, providing the critical values of the remote load and the crack angle/length as functions of a dimensionless structural parameter and of the inclusion radius. The latter functions are in fact representations of the predicted size effect studied in Section 6.

2 Constants for isotropic bimaterials

Following Dundurs (1969) the stress solution of a wide class of elastic plane strain problems for piecewise homogeneous isotropic bimaterials depends only on two dimensionless parameters:

$$\alpha = \frac{\mu_1(\kappa_2+1) - \mu_2(\kappa_1+1)}{\mu_1(\kappa_2+1) + \mu_2(\kappa_1+1)} = \frac{E_1' - E_2'}{E_1' + E_2'}, \tag{1}$$

$$\beta = \frac{\mu_1(\kappa_2-1) - \mu_2(\kappa_1-1)}{\mu_1(\kappa_2+1) + \mu_2(\kappa_1+1)}, \tag{2}$$

where $\mu_k = 0.5E_k/(1+\nu_k)$ and $\kappa_k = 3 - 4\nu_k$ are the shear modulus and the Kolosov's constant of material $k = 1, 2$, with E_k and ν_k denoting the Young elasticity modulus and Poisson ratio, respectively. Effective elasticity modulus is defined as $E_k' = E_k/(1-\nu_k^2)$, and the harmonic mean of the effective elasticity moduli as

$$\frac{1}{E^*} = \frac{1}{2}\left(\frac{1}{E_1'} + \frac{1}{E_2'}\right). \tag{3}$$

Physically admissible values of α and β are restricted to a parallelogram in (α, β) plane enclosed by lines defined as $\alpha = \pm 1$, and by $4\beta = \alpha \pm 1$. Hence, $|\alpha| \leq 1$ and $|\beta| \leq 0.5$.

The so-called oscillation index

$$\varepsilon = \frac{1}{2\pi} \ln \frac{1-\beta}{1+\beta} \tag{4}$$

appears in the elastic solution for an interface crack. Notice that $\cosh^{-2}(\pi\varepsilon) = 1 - \beta^2$.

Two bimaterial systems, representing typical fibre reinforced composites, will be used as examples in the present work: glass fibre/epoxy resin and carbon fibre[1]/epoxy resin, see Table 1 and París et al. (2007). For illustration purposes, other bimaterial systems with extreme values of the Dundurs constants will be considered if useful.

Bimaterial	E_1 (GPa)	ν_1	E_2 (GPa)	ν_2	α	β	ε	E^* (GPa)
glass/epoxy	70.8	0.22	2.79	0.33	0.919	0.229	-0.074	6.01
carbon/epoxy	13.0	0.20	2.79	0.33	0.624	0.136	-0.044	5.09

Table 1: Examples of isotropic bimaterial constants (1 - inclusion, 2 - matrix).

3 Stresses in a single inclusion under a remote transverse tension

Consider an infinitely long cylindrical inclusion, with a circular transversal section, embedded in an infinite matrix and perfectly bonded along its lateral surface. Both inclusion and matrix are assumed to be linearly elastic and isotropic materials identified by numbers 1 and 2 respectively. A uniform uniaxial remote tension $\sigma^\infty > 0$ is applied perpendicularly to the inclusion direction. Thus, a plane strain state is generated in both inclusion and matrix. Let (x, y, z) and (r, θ, z) be suitably defined cartesian and cylindrical coordinate systems, the z-axis being coincident with the inclusion (longitudinal) axis and the x-axis being parallel to the load direction, see Figure 1.

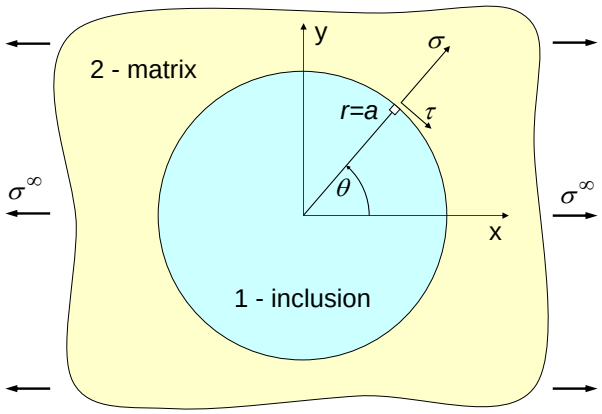

Figure 1: The inclusion problem configuration.

An analytic solution for stresses in this problem was deduced by Goodier (1933). As shown by Hardiman (1954), the stresses inside the inclusion, denoted here as $\sigma_{ij}^{(1)}$, are constant. A compact expression of these stresses was presented by Honein and Herrmann (1990), using two bimaterial constants. Rewriting the aforementioned expression in terms of the Dundurs bimaterial constants α and β gives[2]

$$\begin{pmatrix} \sigma_x^{(1)} & \sigma_{xy}^{(1)} \\ \sigma_{xy}^{(1)} & \sigma_y^{(1)} \end{pmatrix} = \frac{\sigma^\infty}{2} \frac{1+\alpha}{1+\beta} \frac{1}{1+\alpha-2\beta} \begin{pmatrix} 2+\alpha-\beta & 0 \\ 0 & 3\beta-\alpha \end{pmatrix}. \tag{5}$$

[1]The carbon fibre is in fact transversely isotropic. Nevertheless, for a plane strain state, *equivalent isotropic* Young elasticity modulus E and Poisson ratio ν (appearing in Table 1) can be defined in the transversal isotropy plane as follows. Let the coordinate plane 12 be the plane of transversal isotropy, and the axis 3 the rotational symmetry axis. The elastic constants of the carbon fibre assumed are (in this footnote, subscripts denote axes): $\hat{E}_1 = \hat{E}_2 = 13.5$GPa, $\hat{E}_3 = 201$GPa, $\hat{\nu}_{31} = 0.22$ and $\hat{\nu}_{12} = 0.25$. Then, considering a plane strain state, first the effective elasticity modulus and Poisson ratio are defined as $E' = \hat{E}_1/(1-\hat{\nu}_{13}\hat{\nu}_{31})$ and $\nu' = (\hat{\nu}_{12}+\hat{\nu}_{13}\hat{\nu}_{31})/(1-\hat{\nu}_{13}\hat{\nu}_{31})$. Then, using definitions $E' = E/(1-\nu^2)$ and $\nu' = \nu/(1-\nu)$, the equivalent isotropic Young elasticity modulus and Poisson ratio in the transversal isotropy plane are evaluated as $E = \hat{E}_1(1+2\hat{\nu}_{12}+\hat{\nu}_{13}\hat{\nu}_{31})/(1+\hat{\nu}_{12})^2$ and $\nu = (\hat{\nu}_{12}+\hat{\nu}_{13}\hat{\nu}_{31})/(1+\hat{\nu}_{12})$. These equivalent isotropic constants for the carbon fibre, E and ν, will be used hereinafter in the present work.

[2]The bimaterial constants α_{HH} and β_{HH} used by Honein and Herrmann (1990) can be expressed as $\alpha_{HH} = -\frac{\alpha+\beta}{1-\beta}$ and $\beta_{HH} = -\frac{\alpha-\beta}{1+\beta}$.

According to the bounds for α and β, $(2+\alpha-\beta)>0$ and $(1+\alpha-2\beta)\geq 0$ (the equality holds only in the limit case $\alpha=-1$ and $\beta=0$), whereas the expression $3\beta-\alpha$ can be positive or negative.

From (5), normal and tangential tractions, σ and τ, acting along the inclusion/matrix interface ($r=a$), can be easily expressed as functions of the polar angle θ,

$$\sigma(\theta)=\sigma_r(\theta)=\sigma^{\infty}\left(k-m\sin^2\theta\right), \qquad \tau(\theta)=-\sigma_{r\theta}(\theta)=\sigma^{\infty}m\sin\theta\cos\theta, \tag{6}$$

where[3]

$$k(\alpha,\beta)=\frac{1}{2}\frac{1+\alpha}{1+\beta}\frac{2+\alpha-\beta}{1+\alpha-2\beta}\geq 0, \qquad m(\alpha,\beta)=\frac{1+\alpha}{1+\beta}\geq 0. \tag{7}$$

Looking at the left expression in (6), $k(\alpha,\beta)$ can be seen as the concentration factor of the normal tractions defined along the inclusion/matrix interface, their maximum being achieved for $\theta=0$. Thus, it is useful to check its behaviour, shown in Figure 2, as a function of α and β. In the particular case of equal inclusion and matrix materials, $k(0,0)=1$. For $\alpha>0$ and $\beta>0$ (the case the present work is focused on), $k>1$, whereas for $\alpha<0$ and $\beta<0$, $k<1$. The maximum value is $k(1,0.5)=\frac{5}{3}=1.\bar{6}$. The minimum value $k(-1,\beta)=0$ is achieved if $E_1'=0$, the inclusion in fact representing a void. A discontinuity of k can be observed at the point $(\alpha,\beta)=(-1,0)$, where the limits of k take values between 0 and 1 depending on the direction approaching this point.

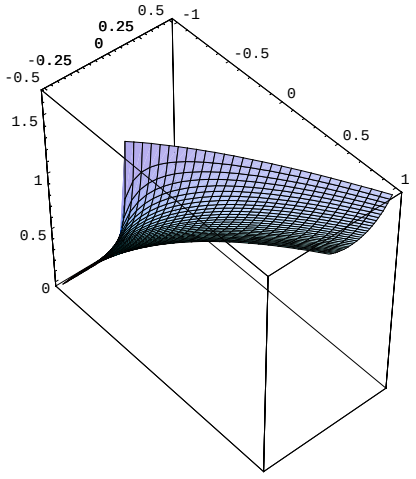

Figure 2: k as a function of α and β in the Dundurs parallelogram.

The behaviour of $m(\alpha,\beta)$, defined by the right expression in (7), is easier to characterize: $m=1$ for $\alpha=\beta$ and $m\lessgtr 1$ for $\alpha\lessgtr\beta$. The maximum and minimum values are $m(1,0)=2$ and $m(-1,\beta)=0$, respectively.

It is instructive to rewrite $\sigma_{ij}^{(1)}$ in (5) in terms of k and m as

$$\begin{pmatrix}\sigma_x^{(1)} & \sigma_{xy}^{(1)}\\ \sigma_{xy}^{(1)} & \sigma_y^{(1)}\end{pmatrix}=\sigma^{\infty}m\begin{pmatrix}\frac{k}{m} & 0\\ 0 & \frac{k}{m}-1\end{pmatrix}. \tag{8}$$

This expressions shows that the character of the inclusion stress state is basically determinate by the ratio $\frac{k}{m}$, in particular when referring to the position of its Mohr circumference with respect to the vertical τ axis.

Let $\alpha>-1$, and consequently $k>0$ and $m>0$. Then, the angle θ_0 for which the interface normal traction vanishes, i.e. $\sigma(\theta_0)=0$, is given by

$$\theta_0(\alpha,\beta)=\arcsin\sqrt{\frac{k}{m}}. \tag{9}$$

The expression on the right hand side of (9) makes sense only if $k\leq m$, which is equivalent to the condition $\sigma_y^{(1)}\leq 0$ or, in terms of the Dundurs constants, to $3\beta\leq\alpha$ and $\alpha>-1$. It will be convenient to define θ_0 for $k>m$ as $\theta_0=\infty$.

[3]For the sake of simplicity, the dependence of different functions on bimaterial or adjustable parameters will be shown explicitly where the function is defined for the first time, but in subsequent usage of these functions these parameters will usually be omitted.

According to the left expression in (6), see also (8), in inclusion/matrix bimaterial systems for which $k > m$, only positive normal tractions take place along the whole interface, which at first sight can be a surprising result. Again, in view of the importance of the ratio $\frac{k}{m}$ for the interface traction distribution it seems useful to check its behaviour, shown in Figure 3, as a function of α and β. It is easy to check analytically that the ratio $\frac{k}{m}$ is unbounded ($\frac{k}{m} \to \infty$) at the corner point $(\alpha, \beta) = (-1, 0)$ of the Dundurs parallelogram, whereas its minimum value $\frac{k}{m} = \frac{3}{4}$ is achieved at the side $4\beta = \alpha - 1$ of this parallelogram. The latter result implies that θ_0 defined in (9) has a minimum value $\theta_0(\alpha, 0.25(\alpha - 1)) = \arcsin \frac{\sqrt{3}}{2} = 60^\circ$. Hence,

$$60^\circ \leq \theta_0 \leq 90^\circ, \qquad \text{for } k \leq m. \tag{10}$$

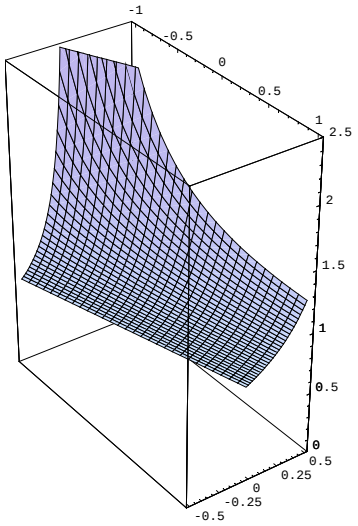

Figure 3: $\frac{k}{m}$ as a function of α and β in the Dundurs parallelogram.

For the bimaterials defined in Table 1, the values of the above defined constants characterizing the inclusion/matrix interface traction distribution are presented in Table 2. In view of (9), very similar values of ratio $\frac{k}{m}$, shown in Table 2, imply that the values of θ_0 for these bimaterials are also very similar.

Bimaterial	k	m	k/m	θ_0 [°]
glass/epoxy	1.44	1.56	0.9205	73.63
carbon/epoxy	1.32	1.43	0.9200	73.57

Table 2: The values of k, m, $\frac{k}{m}$ and θ_0 for the examples of isotropic bimaterials.

4 The solution for a crack at the interface of a single inclusion under a remote transverse tension

Consider now the single inclusion problem configuration from the previous section altered by the presence of a debond—interface crack, symmetrically situated with respect to the load direction, with a semidebond angle ($\theta_d \geq 0$) and an infinite length in the z-axis direction, see Figure 4.

This problem has been studied analytically and numerically by many authors, using both basic models of Interface Fracture Mechanics (open model and contact model), see París et al. (2007) for a review. A fully analytic solution of this problem (in fact of a more general problem) was deduced by Toya (1974), using the open model. A concise presentation and a parametric analysis of the Toya's solution can be found in Murakami (1988). Toya's general expressions for the interface tractions ahead of the crack tip and for the Energy Release

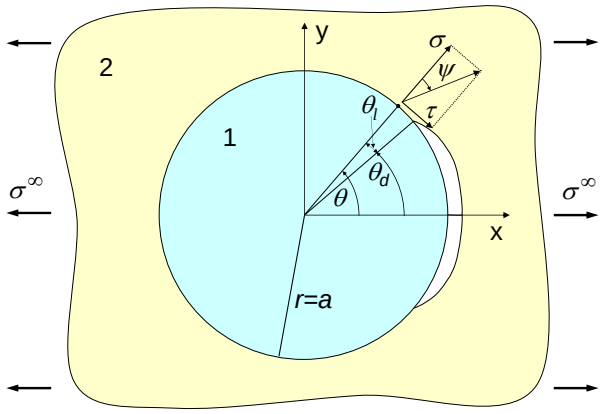

Figure 4: The interface crack problem configuration.

Rate (ERR) are particularized here for the present problem and newly rewritten in terms of the bimaterial constants[4] defined in Section 2. These expressions will be later used in Section 5.

The interface tractions at a point placed ahead of the crack tip at the polar angle $\theta = \theta_d + \theta_\ell$, where $\theta_\ell > 0$, can be evaluated by the complex variable expression:

$$\sigma(\theta) - i\tau(\theta) = -\frac{\sigma^\infty}{2}\frac{1-\alpha}{1-\beta}\chi(\theta)p(\theta), \tag{11}$$

where $i = \sqrt{-1}$ is the imaginary unit, and

$$\chi(\theta) = \left(e^{i\theta} - e^{i\theta_d}\right)^{-\frac{1}{2}-i\varepsilon}\left(e^{i\theta} - e^{-i\theta_d}\right)^{-\frac{1}{2}+i\varepsilon}, \tag{12}$$

$$p(\theta) = q(\theta_d)\left(e^{i\theta} - (\cos\theta_d - 2\varepsilon\sin\theta_d)\right) - \frac{1+\alpha}{1-\alpha}e^{-2\varepsilon(\theta_d-\pi)}\left((\cos\theta_d + 2\varepsilon\sin\theta_d)e^{-i\theta} - e^{-2i\theta}\right), \tag{13}$$

with

$$q(\theta_d) = \frac{1 - (\cos\theta_d - 2\varepsilon\sin\theta_d)e^{2\varepsilon(\theta_d-\pi)} + \frac{1}{2}(1+\alpha)(1+4\varepsilon^2)\sin^2\theta_d}{3+\alpha-(1-\alpha)(\cos\theta_d - 2\varepsilon\sin\theta_d)e^{2\varepsilon(\theta_d-\pi)}} - \frac{1}{1-\alpha}. \tag{14}$$

The ratio of the interface shear and normal tractions ahead of the crack tip at a small (either geometry- or material-based) reference length ℓ gives a measure of fracture mode mixity of an interface crack, see Rice (1988); Hutchinson and Suo (1992); Banks-Sills and Ashkenazi (2000); Mantič and París (2004). An approach to experimentally determine a material-based characteristic reference length ℓ_m has recently been proposed by Agrawal and Karlsson (2007) and discussed by Mantič (2008). Nevertheless, in the present study it seems appropriate to adopt a small geometry-based reference length defined as $\ell_g = \theta_\ell a$, where θ_ℓ is a small fixed reference angle (independent of the debond angle θ_d).

Thus, it will be assumed that the angle ψ given by

$$\tan\psi(\theta_d;\theta_\ell) = \frac{\tau(\theta_d+\theta_\ell)}{\sigma(\theta_d+\theta_\ell)}, \tag{15}$$

provides a suitable measure of the fracture mode mixity. Figure 5 shows the evolution of $\psi(\theta_d)$ for the bimaterials defined in Table 1, considering $\theta_\ell = 0.1°$. Taking different values of θ_ℓ, e.g. $\theta_\ell = 0.01°$ or $1°$ also considered in Section 5.3, would result in curves of the function $\psi(\theta_d)$ similar to those shown in Figure 5, with the straight part shifted an angle.

It should also be noticed that interface tractions ahead of the crack tip, given by (11), and consequently also the angle $\psi(\theta_d)$, are independent of the inclusion radius a.

The ERR of the interface crack propagating, for example, at its upper crack tip at an angle θ_d along the interface can be expressed as

$$G(\theta_d) = \frac{(\sigma^\infty)^2 a}{E^*}\widehat{G}(\theta_d;\alpha,\beta), \tag{16}$$

[4]The bimaterial constants ν_T, β_T, k_T and λ_T used by Toya (1974) can be expressed as $\nu_T = \frac{1-\beta}{1+\beta}$, $\beta_T = \frac{1-\alpha}{1+\beta}$, $k_T = \frac{1-\alpha}{2}$ and $\lambda_T = -\varepsilon$.

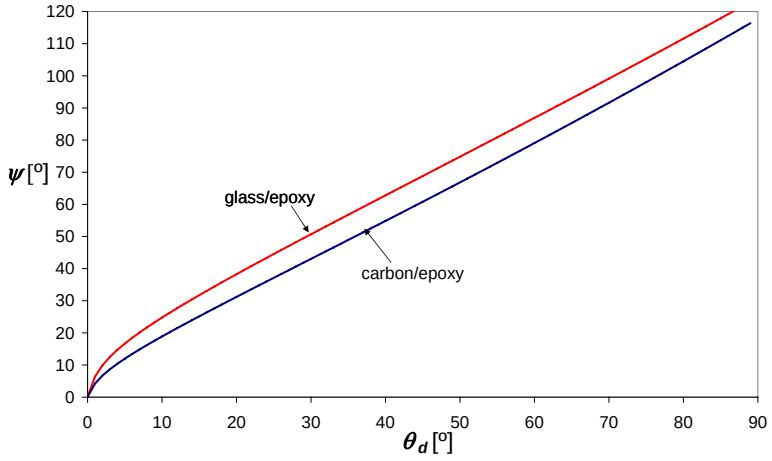

Figure 5: Examples of the evolution of the fracture mode mixity angle ψ taking $\theta_\ell = 0.1°$.

where the dimensionless function $\widehat{G}$ (defining a normalized form of ERR) depends only on θ_d, α and β. It is defined as

$$\widehat{G}(\theta_d;\alpha,\beta) = \pi\left(1+4\varepsilon^2\right)(1+\alpha)^2\sin\theta_d\left(d(\theta_d)(d(\theta_d)-2c(\theta_d)\cos\theta_d)+c(\theta_d)^2\right)/8c(\theta_d), \tag{17}$$

and

$$c(\theta_d) = 2e^{-2\varepsilon(\theta_d-\pi)}, \tag{18}$$

$$d(\theta_d) = -\frac{4-(1-\alpha)(1+4\varepsilon^2)\sin^2\theta_d}{3+\alpha-(1-\alpha)(\cos\theta_d-2\varepsilon\sin\theta_d)e^{2\varepsilon(\theta_d-\pi)}}. \tag{19}$$

It should be noticed that, according to (16), the ERR $G(\theta_d)$ varies linearly with the inclusion radius a.

Sometimes it is useful to approximate $\widehat{G}(\theta_d)$ for small values of θ_d by its Taylor series expansion at $\theta_d = 0$:

$$\widehat{G}(\theta_d) = \left.\frac{\mathrm{d}\widehat{G}}{\mathrm{d}\theta_d}\right|_{\theta_d=0}\theta_d + O(\theta_d^2), \tag{20}$$

where the fact that ERR vanishes for an infinitesimal crack extension, $\widehat{G}(0)=0$, has been taken into account. From (17) it can be shown that

$$\widehat{G}'(0;\alpha,\beta) \overset{\text{def}}{=} \left.\frac{\mathrm{d}\widehat{G}}{\mathrm{d}\theta_d}\right|_{\theta_d=0} = \frac{k^2\pi(1+4\varepsilon^2)}{\cosh^2(\pi\varepsilon)}. \tag{21}$$

Then the derivative of G with respect to the crack semilength, evaluated for the infinitesimal crack length, is expressed as

$$\left.\frac{\mathrm{d}G}{\mathrm{d}(a\theta_d)}\right|_{\theta_d=0} = \frac{(k\sigma^\infty)^2\pi(1+4\varepsilon^2)}{E^*\cosh^2(\pi\varepsilon)}. \tag{22}$$

This expression agrees with the analogous derivative of ERR for a crack at a straight interface between two half-spaces, see Rice (1988), except the factor k^2. In fact, this result could be expected as $k\sigma^\infty$ is the value of the normal tractions acting at $\theta = 0$ before the infinitesimal crack appears therein.

Figure 6 shows evolution of $\widehat{G}(\theta_d)$ and its first order Taylor series expansion, obtained from (21), for the bimaterials defined in Table 1.

5 Interface crack onset at a single inclusion under a remote transverse tension.

A novel approach to solve the problem of a crack onset at a stress concentration (e.g. a blunt notch) or at a weak stress singularity (e.g. a reentrant corner with traction free faces), where originally there is no crack, has

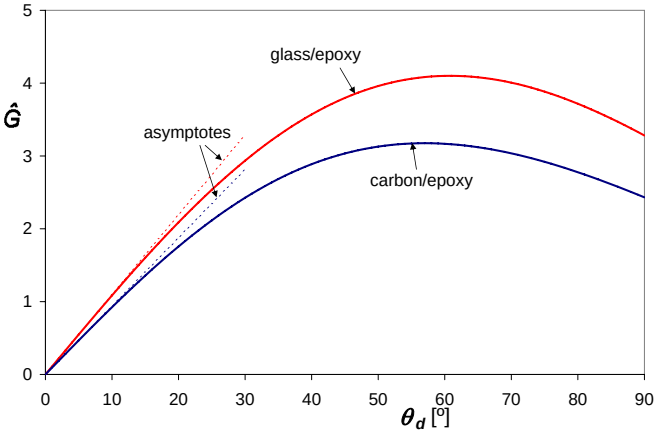

Figure 6: Examples of the evolution of the normalized ERR and its linear approximation.

been developed by Leguillon (2002); Leguillon and Siruguet (2002); Leguillon et al. (2007) in the framework of Finite Fracture Mechanics. The key idea of this approach is to use two coupled criteria, one strength based and one energy based, either of them representing a necessary but not sufficient condition for the crack onset. Applying each criterion individually leads to unresolvable questions, requiring the definition of a characteristic length, in the following sense:

- The stress-strength criterion determines the minimum value of the applied load leading to rupture, but it is unable to determine unambiguously the size of the crack originated.
- An application of the (infinitesimal) Griffith type energy criterion for crack growth requires an a priori existing crack. Therefore, no fundament for determining the initial crack length is given.

However, when assuming an abrupt onset of a crack of a finite length, and applying both criteria simultaneously, they provide a system of two (typically nonlinear) equations for two unknowns: the length of the crack originated and the critical load required for its onset.

In what follows, a generalization of the Leguillon's coupled criterion for the interface cracks, where the fracture toughness is a function of fracture mode mixity, is applied to the present problem of the interface crack onset at a single circular cylindrical inclusion embedded in a matrix subjected to a remote transverse uniaxial tension.

5.1 Tensile stress criterion

A stress criterion is usually invoked if no pre-existing debond exists at the inclusion surface. The tensile stress criterion adopted here assumes the existence of a critical value $\sigma_c > 0$ of interface normal tensions—interfacial tensile strength, defined as the maximum tension that the interface can sustain without fracture. Thus, according to this stress criterion, the inclusion/matrix interface will break at those points where tension exceeds σ_c:

$$\sigma(\theta) \geq \sigma_c. \tag{23}$$

In the present problem of remote uniaxial tension, the normal stress $\sigma(\theta)$ is changing along the interface with the position angle θ as shown in (6). Combining the left expression in (6) with (23) leads to the necessary condition for rupture at an interface point defined by the angle θ:

$$\frac{\sigma^\infty}{\sigma_c} \geq \frac{1}{k - m\sin^2\theta}. \tag{24}$$

Inasmuch as the function on the right hand side of (24) increases with increasing $|\theta|$, the interface debond is expected to happen, for a sufficiently large particular value of ratio σ^∞/σ_c, along the entire portion of the inclusion surface, symmetrically with respect to the load direction, limited by the maximum angle θ_c^σ for which (24), and equivalently the stress criterion (23), are fulfilled,

$$|\theta| \leq \theta_c^\sigma. \tag{25}$$

Maximum angle $\theta_c^\sigma \geq 0$ is well defined, and any interface breakage can be expected, if and only if a sufficiently large remote tension σ^∞ is applied, providing that the following condition holds:

$$\frac{\sigma^\infty}{\sigma_c} \geq k^{-1}. \tag{26}$$

Then, assuming (26), θ_c^σ is defined as

$$\theta_c^\sigma\left(\frac{\sigma^\infty}{\sigma_c};\alpha,\beta\right) = \begin{cases} \arcsin\sqrt{\frac{k}{m}\left(1-\frac{\sigma_c}{k\sigma^\infty}\right)}, & k \leq m, \text{ or } k > m \text{ and } \frac{\sigma^\infty}{\sigma_c} \leq \frac{1}{k-m}, \\ 180°, & k > m \text{ and } \frac{\sigma^\infty}{\sigma_c} > \frac{1}{k-m}. \end{cases} \tag{27}$$

The function in the first row on the right hand side of (27) is obtained by solving the equality in (24). The second row in (27) indicates that for $k > m$ and a sufficiently large remote tension the stress criterion predicts the complete debonding of the inclusion.

If $k \leq m$, then there is an upper bound for θ_c^σ given by θ_0 defined in (9). Hence,

$$\theta_c^\sigma < \theta_0(\alpha,\beta) = \arcsin\sqrt{\frac{k}{m}}. \tag{28}$$

A graphical representation of the stress criterion for the bimaterials defined in Table 1, an extremal bimaterial system with $(\alpha,\beta) = (1, 0.5)$ giving $\frac{k}{m} = 1.25$, and for $\frac{k}{m} = 1$, corresponding e.g. to $(\alpha,\beta) = (1, 0.\bar{3})$, is shown in Figure 7. The plotted curves define θ_c^σ for a given normalized remote load $\frac{\sigma_c}{\sigma^\infty}$ according to (27), the traditional meaning of the horizontal and vertical axes being altered thinking of the application of these curves in the following sections. An alternative interpretation of these curves, according to criterion (24), is also useful. In simple terms, points placed over the stress criterion curve in Figure 7 correspond to the interface rupture predicted, whereas points below this curve are in the safe zone.

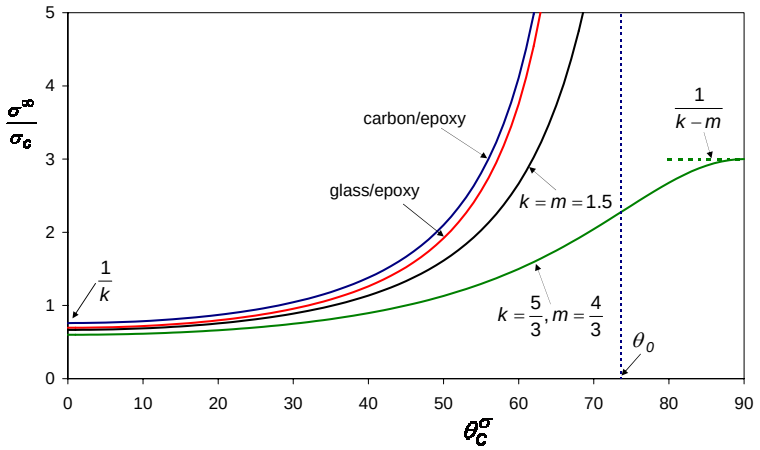

Figure 7: Graphical representation of the stress criterion.

One can realize from the above analysis, and in particular from (27), that the stress criterion alone is not sufficient to unambiguously predict the critical value of the remote load σ_c^∞ for which the interface debond will occur, or equivalently which portion of the inclusion surface, defined by $|\theta| \leq \theta_c^\sigma$, will initially debond. The reason is that it provides only one equation for two unknowns, σ_c^∞ and θ_c^σ.

5.2 Incremental energy criterion

The incremental Griffith criterion adopted here is based on an energy balance between an elastic initial state prior to a crack onset and after the appearance of a finite crack of an angle $2\Delta\theta > 0$. The term 'incremental' refers to 'a finite increment of the crack length' here, as opposed to the classical assumption of 'an infinitesimal increment of the crack length'. On the assumption of a constant interface fracture toughness G_c, this energy balance would be written as:

$$\Delta\Pi + \Delta E_k + G_c\, a2\Delta\theta = 0, \tag{29}$$

where $\Delta\Pi$ is the change in potential energy and ΔE_k is the change in kinetic energy.

However, the previous assumption of a constant interface fracture toughness G_c does not seem to be realistic in the present case of an interface crack onset. The fracture mode mixity at the tip of a hypothetical crack situated along the inclusion/matrix interface significantly depends on the crack angle $2\theta_d$, as described by the evolution of the angle $\psi(\theta_d)$ in Figure 5. It is well known, see Hutchinson and Suo (1992); Gerberich and Yang (2003); Mantič et al. (2006), that such variations of fracture mode mixity in an interface crack are usually associated to relevant variations of interface fracture toughness. In fact, G_c is considered as a function of ψ, $G_c(\psi)$, characterizing a particular bimaterial interface and being represented by the so called toughness curve. Hutchinson and Suo (1992) proposed the following phenomenological law:

$$G_c(\psi; G_{1c}, \lambda, \psi_0) = G_{1c}\left(1 + \tan^2[(1-\lambda)(\psi - \psi_0)]\right), \tag{30}$$

which is widely accepted as a reasonable approximation of a real toughness curve. In (30), G_{1c} is considered as the fracture Mode I toughness (also called separation energy, associated to the minimum value of $G_c(\psi)$). λ is a fracture mode-sensitivity parameter, whose value can be adjusted to fit experimental data, e.g. typical range $0.2 \leq \lambda \leq 0.35$ characterizes interfaces with moderately strong fracture mode dependence. Finally, ψ_0 is a phase shift, which can be modified by taking a different reference angle θ_ℓ defining the distance from the crack tip where ψ is evaluated, see (15). Thus, hereinafter, without loss of generality $\psi_0 = 0$ will be assumed. Figure 8 shows distributions of the interface fracture toughness as a function of θ_d, $G_c(\psi(\theta_d; \theta_\ell); G_{1c}, \lambda)$, obtained combining the distributions of $\psi(\theta_d)$ shown in Figure 5 and (30), for the bimaterials defined in Table 1, taking $\lambda = 0.3$ and a small reference angle $\theta_\ell = 0.1°$.

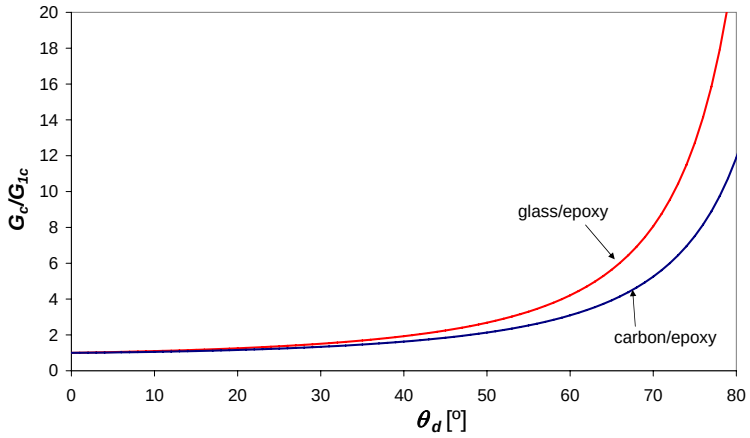

Figure 8: Examples of the normalized interface fracture toughness curves $G_c(\psi(\theta_d))/G_{1c}$, taking $\lambda = 0.3$ and $\theta_\ell = 0.1°$.

According to the previous discussion, the following generalized form of the energy balance seems to be better suited than (29) for the present case of an interface crack onset at the inclusion/matrix interface:

$$\Delta\Pi + \Delta E_k + \int_0^{\Delta\theta} G_c(\psi(\theta_d)) 2a \mathrm{d}\theta_d = 0, \tag{31}$$

where the integral term gives the total energy required to originate an interface crack of an angle $2\Delta\theta$ symmetrically situated around $\theta = 0$.

If the initial state is quasi-static, then there is a production of kinetic energy, $\Delta E_k \geq 0$, and the above energy balance leads to the inequality:

$$-\Delta\Pi \geq \int_0^{\Delta\theta} G_c(\psi(\theta_d)) 2a \mathrm{d}\theta_d. \tag{32}$$

Recall the relation, known from classical (differential) Fracture Mechanics, between the (differential) Energy Release Rate (ERR) and the derivative of the potential energy with respect to the crack length,

$$G(\theta_d) = -\frac{\mathrm{d}\Pi}{\mathrm{d}(2a\theta_d)}. \tag{33}$$

Then, the finite variation of the potential energy $\Delta\Pi$ can be evaluated as follows:

$$-\Delta\Pi = -\int_0^{\Delta\theta} \frac{\mathrm{d}\Pi}{\mathrm{d}(2a\theta_d)} 2a\mathrm{d}\theta_d = \int_0^{\Delta\theta} G(\theta_d) 2a\mathrm{d}\theta_d. \tag{34}$$

Combining (32) with (34) gives the necessary energetic condition for the onset of a crack of length $2a\Delta\theta$ at the (originally undamaged) inclusion/matrix interface:

$$\int_0^{\Delta\theta} G(\theta_d)\mathrm{d}\theta_d \geq \int_0^{\Delta\theta} G_c(\psi(\theta_d))\mathrm{d}\theta_d. \tag{35}$$

The term on the left hand side in (35) corresponds to the energy available to be released during the interface crack onset, whereas the term on the right hand side corresponds to the energy required for such a crack onset. Recall that only a crack symmetric with respect to the angle $\theta = 0$ is considered here. Notice that in contrast with the corresponding classical Griffith condition, the inequality (35) involves an a priori unknown and finite crack angle increment $\Delta\theta$.

Considering that $G(0) = 0$ and $G_c(\psi(0)) > 0$, there exists a minimum angle $\theta_c^E > 0$ for which the condition (35) is fulfilled. Consequently, (35) is not valid for any $\Delta\theta < \theta_c^E$, while it holds for a range of $\Delta\theta \geq \theta_c^E$, not being valid for large values of $\Delta\theta$ due to a strong increase of G_c, shown in Figure 8, and a decreasing character of G after achieving its maximum, see Figure 6.

By substituting relationships (16) and (30) into (35), and after a rearrangement, this necessary energetic condition writes as:

$$\frac{(\sigma^\infty)^2\, a}{G_{1c}E^*} \geq g(\Delta\theta), \tag{36}$$

where

$$g(\Delta\theta;\alpha,\beta;\lambda,\theta_\ell) = \frac{\int_0^{\Delta\theta} \left(1+\tan^2[(1-\lambda)\psi(\theta_d)]\right)\mathrm{d}\theta_d}{\int_0^{\Delta\theta} \widehat{G}(\theta_d)\mathrm{d}\theta_d} > 0, \tag{37}$$

is a universal dimensionless function of $\Delta\theta > 0$. Note that, as indicated on the left-hand side of (37), in addition to the Dundurs parameters, g also depends, in a secondary manner, on the chosen values of the parameters λ and θ_ℓ.

Figure 9 shows the function $g(\Delta\theta)$ for the examples of bimaterials defined in Table 1. The integrals of smooth functions appearing in definition (37) can be efficiently computed by usual numerical quadratures.

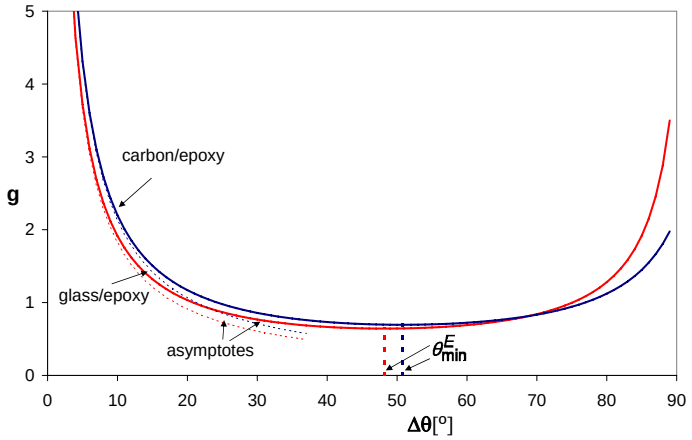

Figure 9: Universal dimensionless function $g(\Delta\theta)$, taking $\lambda = 0.3$ and $\theta_\ell = 0.1°$.

As can be expected from the behaviour of the functions integrated on the right hand side of (37), and as observed in Figure 9, the function $g(\Delta\theta)$ has a minimum achieved at an angle denoted as

$$\theta_{\min}^E(\alpha,\beta;\lambda,\theta_\ell) > 0. \tag{38}$$

As will be seen later, $\theta_{\min}^E$ plays a key role in the characterization of the crack onset under study. Moreover, it will be seen that the shape of the branch of $g(\Delta\theta)$ for $\Delta\theta > \theta_{\min}^E$ is in fact not relevant for the interface crack onset predictions presented.

It will be useful to observe that the logarithmic derivative of the function $g(\Delta\theta)$ can be expressed (using the definitions (16), (30) and (37)) by:

$$\frac{\mathrm{d}\log g}{\mathrm{d}\Delta\theta}=\frac{1}{g(\Delta\theta)}\frac{\mathrm{d}g}{\mathrm{d}\Delta\theta}=\frac{G_c(\psi(\Delta\theta))}{\int_0^{\Delta\theta}G_c(\psi(\theta_d))\mathrm{d}\theta_d}-\frac{G(\Delta\theta)}{\int_0^{\Delta\theta}G(\theta_d)\mathrm{d}\theta_d}\begin{cases}<0, & \text{for } \Delta\theta<\theta^E_{\min},\\ =0, & \text{for } \Delta\theta=\theta^E_{\min},\\ >0, & \text{for } \Delta\theta>\theta^E_{\min}.\end{cases} \tag{39}$$

The relationships on the right hand side of (39) follow from the considering the sign of the derivative of g and the fact that $g>0$.

Taking into account that $g(\Delta\theta)$ is a decreasing function for $\Delta\theta<\theta^E_{\min}$, for a sufficiently large particular value of σ^∞ there exists a minimum angle denoted as $\theta^E_c(\sigma^\infty)$, $\theta^E_c\le\theta^E_{\min}$, for which a debond is energetically allowed. θ^E_c is defined by the equality in (36), and subsequently also in (35). Hence, in view of (39),

$$G\left(\theta^E_c\right)>G_c\left(\psi\left(\theta^E_c\right)\right)\quad\text{for}\quad\theta^E_c<\theta^E_{\min},\qquad\text{whereas}\qquad G\left(\theta^E_c\right)=G_c\left(\psi\left(\theta^E_c\right)\right)\quad\text{for}\quad\theta^E_c=\theta^E_{\min}. \tag{40}$$

Moreover, as follows from (39), also

$$G\left(\theta^E_{\min}\right)>G_c\left(\psi\left(\theta^E_{\min}\right)\right)\quad\text{for}\quad\theta^E_c<\theta^E_{\min}. \tag{41}$$

In deduction of (41) the inequality $\int_0^{\theta^E_{\min}}G(\theta_d)\mathrm{d}\theta_d>\int_0^{\theta^E_{\min}}G_c(\psi(\theta_d))\mathrm{d}\theta_d$, obtained from the relations $g(\theta^E_c)>g(\theta^E_{\min})$ and $\int_0^{\theta^E_c}G(\theta_d)\mathrm{d}\theta_d=\int_0^{\theta^E_c}G_c(\psi(\theta_d))\mathrm{d}\theta_d$, has been used.

Obviously, a debond is also energetically allowed for a certain range of $\Delta\theta$, whose lower bound is given by θ^E_c,

$$\theta^E_c\le\Delta\theta, \tag{42}$$

whereas its upper bound (being greater than $\theta^E_{\min}$) depends on the shape of $g(\Delta\theta)$ for $\Delta\theta>\theta^E_{\min}$.

In fact, the existence of a minimum in $g(\Delta\theta)$ at $\Delta\theta=\theta^E_{\min}$ leads to the prediction of the minimum remote tension value $\sigma^{\infty,E}_c$ originating a debond, according to the present incremental energetic criterion (36), as

$$\sigma^{\infty,E}_c=\sqrt{\frac{G_{1c}E^*}{a}g\left(\theta^E_{\min}\right)}. \tag{43}$$

Then, the predicted extension of the debond originated by this remote tension is given by $\Delta\theta=\theta^E_c=\theta^E_{\min}$.

According to the above analysis, in this particular case the following two equalities hold:

$$\int_0^{\theta^E_{\min}}G(\theta_d)\mathrm{d}\theta_d=\int_0^{\theta^E_{\min}}G_c(\psi(\theta_d))\mathrm{d}\theta_d\quad\text{and}\quad G\left(\theta^E_{\min}\right)=G_c\left(\psi\left(\theta^E_{\min}\right)\right). \tag{44}$$

Moreover, as shown in Appendix A,

$$\left.\frac{\mathrm{d}G(\theta_d)}{\mathrm{d}\theta_d}\right|_{\theta_d=\theta^E_c=\theta^E_{\min}}<\left.\frac{\mathrm{d}G_c(\psi(\theta_d))}{\mathrm{d}\theta_d}\right|_{\theta_d=\theta^E_c=\theta^E_{\min}}, \tag{45}$$

which implies, in view of (44), that according to either energy criterion, the incremental or the classical infinitesimal one, no further crack growth after the onset of a crack of a semiangle $\theta^E_{\min}$, originated by the load $\sigma^{\infty,E}_c$, is expected.

The two different situations characterized by the equality in (35), and either by the inequalities or equalities in (40), are illustrated in Figure 10 by examples of the distributions of $G(\theta_d)$ and $G_c(\psi(\theta_d)$ for the glass/epoxy bimaterial defined in Table 1. Areas of the same size corresponding to the two integrals in (35) are indicated in Figure 10 as well. Several other general relationships between G and G_c are illustrated in Figure 10, e.g., Figure 10(a) illustrates the inequality (41), whereas Figure 10(b) illustrates the inequalities (45) (or equivalently (75)) and (73). The following particular values of problem parameters, chosen somewhat arbitrarily, have been used to generate these plots: $a=7.5\mu$m, $\sigma^\infty=80.7$MPa, $G_{1c}=10\mathrm{Jm}^{-2}$ and $\theta^E_c=27.5^\circ$ in Figure 10(a), whereas $G_{1c}=12.6\mathrm{Jm}^{-2}$ and $\theta^E_c=\theta^E_{\min}=48.2^\circ$ in Figure 10(a).

It should be stressed that the remote tension $\sigma^{\infty,E}_c$, which implies that a sufficient amount of energy can be released at the onset of a crack of a semiangle $\theta^E_{\min}$, may not be sufficiently large to guarantee that the normal tractions along the interface portion defined by $|\theta|<\theta^E_{\min}$ are greater than the interface strength. This difficulty will be solved in the next section.

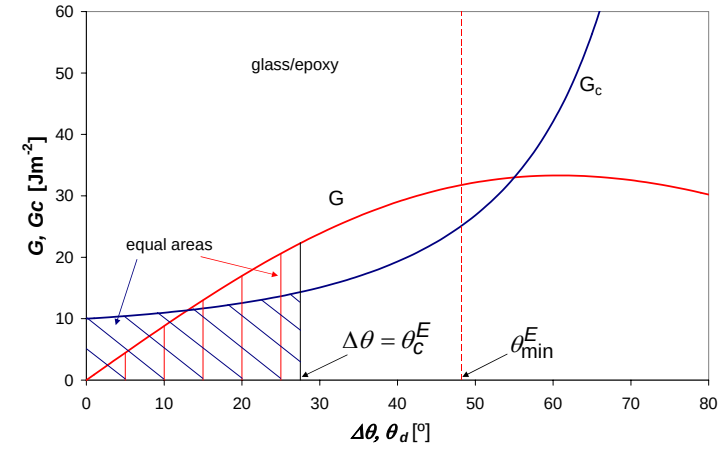

(a)

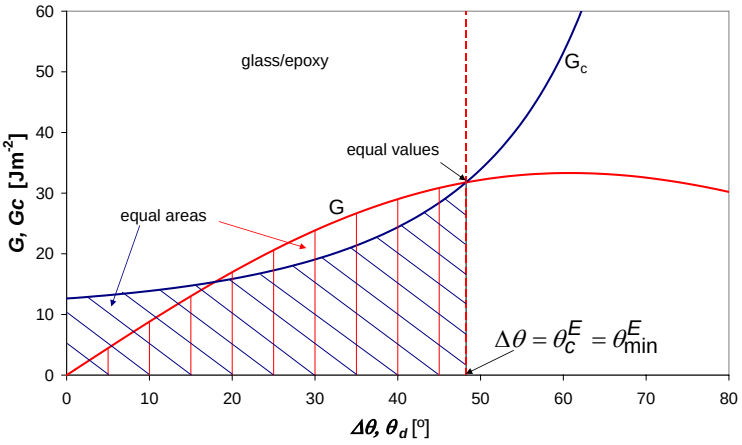

(b)

Figure 10: Examples of the evolutions of the ERR $G(\theta_d)$ and the interface fracture toughness $G_c(\psi(\theta_d))$ (taking $\lambda = 0.3$ and $\theta_\ell = 0.1°$) for the glass/epoxy bimaterial. Cases: (a) $\theta_c^E < \theta_{\min}^E$, (b) $\theta_c^E = \theta_{\min}^E$.

Finally, it will be useful to have a simple approximation of $g(\Delta\theta)$ for small values of $\Delta\theta$. Taking into account that, according to Figure 5, $\psi(\theta_d)$ is small for small θ_d, $\tan^2(1-\lambda)\psi(\theta_d)$ can be considered negligible with respect to the unity in (30), giving $G_c(\psi(\theta_d)) \gtrapprox G_{1c}$ for small θ_d. Then, using the first order Taylor expansion of $\widehat{G}(\theta_d)$ in (20) leads to

$$g(\Delta\theta;\alpha,\beta;\lambda,\theta_\ell) \gtrapprox \tilde{g}(\Delta\theta;\alpha,\beta) = \frac{2}{\widehat{G}'(0;\alpha,\beta)\Delta\theta} \qquad \text{for small} \quad \Delta\theta > 0, \tag{46}$$

where it is indicated that the approximate function $\tilde{g}(\Delta\theta)$, also shown in Figure 9, always underestimates $g(\Delta\theta)$. This is easy derived from the facts that $G_c(\psi) \geq G_{1c}$ and that $G(\theta_d)$ is overestimated by its linear approximation, given by its first order Taylor series expansion at $\theta_d = 0$, as shown in Figure 6. For the bimaterials considered, $\tilde{g}(\Delta\theta)$ reasonably approximates $g(\Delta\theta)$ for $\Delta\theta$ less than $10° - 20°$. Notice, however, that $\tilde{g}(\Delta\theta)$ has no minimum and does not allow $\theta_{\min}^E$ to be estimated.

5.3 Coupled stress and energy criterion

Combining both above described necessary criteria for debond onset, it is obtained that, for a sufficiently large value of σ^∞ (guaranteeing the fulfilment of both criteria), the allowed semidebond angle $\Delta\theta$ should verify:

$$\theta_c^E \leq \Delta\theta, \qquad \text{and} \qquad \Delta\theta \leq \theta_c^\sigma. \tag{47}$$

When decreasing the value of σ^∞, θ_c^E is increasing (see (36) and Figure 9) whereas θ_c^σ is decreasing (see (27)

and Figure 7). Then, the following two scenarios (denoted A and B) are possible, depending on the bimaterial and interface properties and the inclusion size.

In scenario A, a minimum value of σ^∞ is found for which the equality

$$\theta_c \overset{\text{def}}{=} \theta_c^E = \theta_c^\sigma \tag{48}$$

is achieved. Thus, $\theta_c \leq \theta_{\min}^E$.

In scenario B, θ_c^E achieves its upper bound $\theta_{\min}^E$ before becoming equal to θ_c^σ, i.e. it holds that $\theta_c^E < \theta_c^\sigma$. As a further decrease of σ^∞ is not allowed by the energy criterion, then

$$\theta_c \overset{\text{def}}{=} \theta_c^E = \theta_{\min}^E. \tag{49}$$

The critical value of the remote tension σ_c^∞ originating a debond of semiangle

$$\Delta\theta = \theta_c \tag{50}$$

is evaluated, in scenario A, by the following equation, obtained by combining equalities in (24) and in (36):

$$\frac{\sigma_c^\infty}{\sigma_c} = \gamma\sqrt{g(\theta_c)} = \frac{1}{k - m\sin^2\theta_c}, \qquad (\theta_c \leq \theta_{\min}^E) \tag{51}$$

where a new governing dimensionless parameter[5]:

$$\gamma = \frac{1}{\sigma_c}\sqrt{\frac{G_{1c}E^*}{a}} > 0 \tag{52}$$

has been introduced. Parameter γ is a structural parameter, as it depends not only on a bimaterial property E^* and the interface properties G_{1c} and σ_c, but also on the unique characteristic length of the present problem geometry, the inclusion radius a.

In scenario B, σ_c^∞ is evaluated by the expression:

$$\frac{\sigma_c^\infty}{\sigma_c} = \gamma\sqrt{g(\theta_c)} > \frac{1}{k - m\sin^2\theta_c} \qquad (\theta_c = \theta_{\min}^E). \tag{53}$$

The two described scenarios are illustrated, for the bimaterial systems defined in Table 1, in Figure 11, where the values of γ have been arbitrarily chosen, namely $\gamma = 1$ (scenario A) and 5 (scenario B). It can be observed from these plots that $\frac{\sigma_c^\infty}{\sigma_c}$ represents the minimum normalized remote load for which both stress and energy criteria are fulfilled.

According to (40), in scenario A

$$G(\theta_c) > G_c(\psi(\theta_c)), \tag{54}$$

except for the upper limit angle $\theta_c = \theta_{\min}^E$, where the equality holds, whereas in scenario B

$$G(\theta_c) = G_c(\psi(\theta_c)). \tag{55}$$

From the above analysis, the critical values of the semidebond angle and of the remote tension, θ_c and σ_c^∞, can be computed by the procedure outlined in Figure 12. As can be deduced from this procedure and from the plots in Figure 11, while in scenario A the critical values θ_c and σ_c^∞ are computed from the combination of both stress and energy criteria, in scenario B these values are governed by the energy criterion only, the stress criterion then being automatically fulfilled.

[5] Analogous dimensionless parameters for homogeneous materials have previously been introduced by several authors in different contexts, e.g.: the parameter $x = \frac{K_{Ic}}{\sigma_{YS}\sqrt{\pi D}}$ for a circumferentially notched round metallic bar of diameter D, where where K_{Ic} is the material fracture toughness and σ_{YS} is the uniaxial tensile yield stress, by Irwin (1960); the brittleness number s, for linear elastic-perfectly plastic materials defined as $s = \frac{K_{Ic}}{\sigma_y\sqrt{b}}$, where σ_y is the yield strength and b is a characteristic length of the structure, and for brittle and quasibrittle materials defined as $s = \frac{K_{Ic}}{\sigma_u\sqrt{b}}$, where σ_u is the ultimate strength, by Carpinteri (1981, 1982); the Irwin number for ductile materials, $I = \frac{\sigma_y\sqrt{\ell}}{K_c}$, correlated to the the square root of the ratio between a characteristic length of the structure ℓ and the ultimate size of the plastic zone near the crack tip, $\frac{1}{\pi}\frac{K_c^2}{\sigma_y^2}$, by Barenblatt (1993), cf. Irwin (1960). Nevertheless, it seems that the present definition of γ is the first proposal of a dimensionless parameter of this kind for interface cracks. In fact, γ could be considered as a generalization of the Carpinteri's brittleness number s to interface cracks.

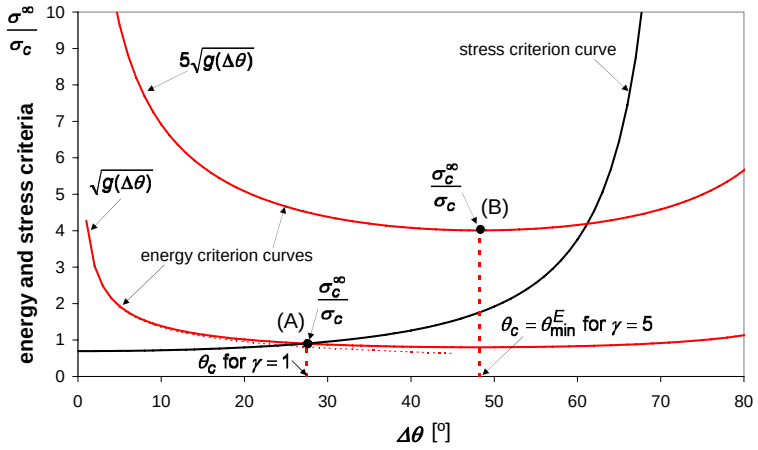

(a)

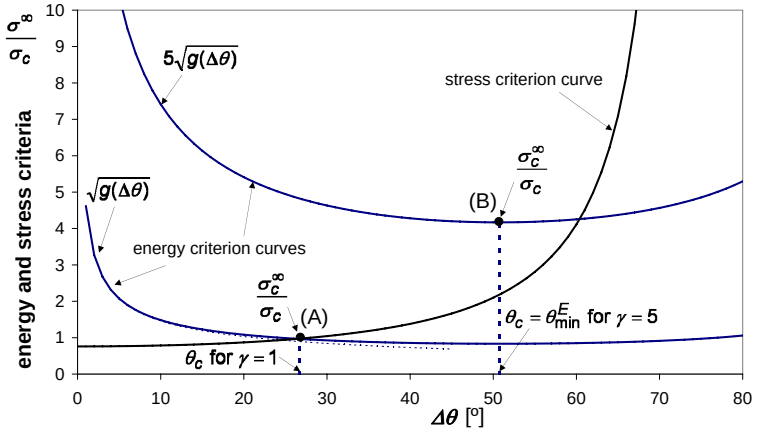

(b)

Figure 11: Plots of coupled stress and energy criteria, scenario A defined by (51) with $\gamma = 1$, and scenario B defined by (53) with $\gamma = 5$, taking $\lambda = 0.3$ and $\theta_\ell = 0.1°$. (a) glass/epoxy, (b) carbon/epoxy.

Let a threshold value of γ be defined as

$$\gamma_{\rm th}(\alpha, \beta; \lambda, \theta_\ell) = \frac{1}{\sqrt{g(\theta^E_{\min})}} \frac{1}{k - m \sin^2 \theta^E_{\min}}. \tag{56}$$

Then, scenario A corresponds to $0 < \gamma \leq \gamma_{\rm th}$. In simple terms, small values of γ are associated to relatively small values of the interface fracture toughness G_{1c} or of the harmonic mean of the effective Young moduli E^*, or to relatively large values of the interface strength σ_c or of the inclusion radius a. It can be deduced from Figure 11 that

$$\lim_{\gamma \to 0_+} \theta_c = 0. \tag{57}$$

Then, θ_c can be approximated by a quadratic function of γ,

$$\theta_c \cong \frac{2k^2}{\widehat{G}'(0)} \gamma^2 = \frac{2 \cosh^2(\pi\varepsilon)}{\pi\,(1 + 4\varepsilon^2)} \gamma^2, \qquad \text{for sufficiently small values of } \gamma > 0, \tag{58}$$

obtained by neglecting $m \sin^2 \theta_c$ with respect to k on the right hand side of (51), and by approximating $g(\theta_c)$ by $\tilde{g}(\theta_c)$ defined in (46). In view of these results, it is obtained from (51) that

$$\frac{\sigma_c^\infty}{\sigma_c} \gtrsim k^{-1}, \qquad \text{for sufficiently small values of } \gamma > 0, \tag{59}$$

σ_c^∞ then being essentially strength governed. Notice that the upper bounds of ranges where (58) and (59) are valid are not sharply defined.

Find $\min_{\Delta\theta} g(\Delta\theta) \stackrel{\text{def}}{=} g(\theta^E_{\min})$

If $\left(\theta^E_{\min} < \theta_0 \text{ and } \gamma\sqrt{g(\theta^E_{\min})} < \frac{1}{k - m\sin^2\theta^E_{\min}}\right)$ or $\theta^E_{\min} \geq \theta_0$ then

Solve the following equation for $\Delta\theta < \min\left\{\theta^E_{\min}, \theta_0\right\}$:

$\gamma\sqrt{g(\Delta\theta)} = \frac{1}{k - m\sin^2\Delta\theta}$

$\theta_c =$the solution $\Delta\theta$ of this equation

Else

$\theta_c = \theta^E_{\min}$

Endif

Compute the critical load σ_c^∞ by

$\frac{\sigma_c^\infty}{\sigma_c} = \gamma\sqrt{g(\theta_c)}$ or equivalently by $\sigma_c^\infty = \sqrt{\frac{G_{1c}E^*}{a}g(\theta_c)}$

End

Figure 12: Computational procedure for the evaluation of θ_c and σ_c^∞.

Scenario B corresponds to $\gamma > \gamma_{\text{th}}$. In simple terms, large values of γ are associated to relatively large values of the interface fracture toughness G_{1c} or of the harmonic mean of the effective Young moduli E^*, or to relatively small values of the interface strength σ_c or of the inclusion radius a. In this case, the interface crack onset is essentially governed by the energy criterion. Then,

$$\theta_c = \theta^E_{\min}, \qquad \text{for } \gamma > \gamma_{\text{th}}, \tag{60}$$

and, in view of (43),

$$\frac{\sigma_c^\infty}{\sigma_c} = \frac{\sigma_c^{\infty,E}}{\sigma_c} = \gamma\sqrt{g(\theta^E_{\min})}, \qquad \text{for } \gamma > \gamma_{\text{th}}. \tag{61}$$

Thus, while θ_c is constant for $\gamma > \gamma_{\text{th}}$, σ_c^∞ is a linear function of γ.

The values of the characteristic parameters $\theta^E_{\min}$, $g(\theta^E_{\min})$ and γ_{th} for the examples of isotropic bimaterials defined in Table 1 are presented in Table 3. To check how the choice of the values of the fracture-mode sensitivity parameter λ, used in (30), and of the reference angle θ_ℓ, used in (15), may affect these characteristic parameters, different values of λ and θ_ℓ are considered in Table 3.

Bimaterial	λ	$\theta^E_{\min}$	$g(\theta^E_{\min})$	γ_{th}
glass/epoxy	0.2	37.7°/42.5°/46.8°	0.92/0.73/0.63	1.2/1.6/2.1
	0.3	43.8°/48.2°/52.3°	0.77/0.64/0.56	1.7/2.2/2.9
carbon/epoxy	0.2	43.0°/45.6°/47.8°	0.85/0.77/0.71	1.7/1.9/2.2
	0.3	48.3°/50.7°/52.7°	0.76/0.70/0.65	2.2/2.6/3.0

Table 3: The values of $\theta^E_{\min}$, $g(\theta^E_{\min})$ and γ_{th} for the examples of isotropic bimaterials, and two values of λ (0.2/0.3) and three values of θ_ℓ (0.01°/0.1°/1°).

The applicability of the Toya (1974) solution for the bimaterials considered can be easily checked by means of a formula, deduced by Hills and Barber (1993) and generalized by Graciani et al. (2007), for the estimation of the extension of the interpenetration zone adjacent to an interface crack tip, always existent in the open model solution. Rewriting this formula to the present case, the angle $\theta_{\text{I}}(\theta_d)$ defining the length of this interpenetration zone can be obtained as the largest value of

$$\theta_{\text{I}}(\theta_d) = \theta_\ell \exp\left[\left\{\left(2n - \frac{1}{2}\right)\pi - \psi(\theta_d;\theta_\ell)\text{sgn}\varepsilon + \arctan(2|\varepsilon|)\right\}/|\varepsilon|\right], \tag{62}$$

which is lower than the debond angle $2\theta_d$, with n being an integer. By substituting into this formula the values of the fracture mode mixity angle ψ computed by (15) (see also Figure 5) and corresponding to the values of θ_ℓ and $\theta_d = \theta^E_{\min}$ from Table 3, it is obtained that for glass/epoxy $\theta_{\text{I}} < 0.052°$, whereas for carbon/epoxy $\theta_{\text{I}} < 0.00046°$. Thus, these interpenetration zones are sufficiently small to validate the open model solution from Toya (1974) in the procedure presented. The fact that $\theta_{\text{I}}(\theta_d)$ is an increasing function of θ_d for the range of θ_d considered has been taken into account in the interpenetration zone estimations.

Figures 13(a) and (b) show θ_c and $\frac{\sigma_c^\infty}{\sigma_c}$ as functions of the dimensionless structural parameter γ for the bimaterials defined in Table 1, taking $\lambda = 0.3$ and $\theta_\ell = 0.1°$. Inasmuch as some features of these functions, in particular the asymptotic behaviour, are more easily identified in log-log scale, the corresponding log-log plots are presented as well, Figure 14. One can easily check from these plots how the variation of one of the problem parameters, e.g. σ_c or G_{1c}, may affect the initial debond angle and the critical remote load value.

According to Table 3, choosing different values of λ and θ_ℓ from physically reasonable ranges results in, at most, moderate variations of the characteristic parameters $\theta^E_{\min}$, $g(\theta^E_{\min})$ and γ_{th}. Thus, also in view of the fact that the asymptotes shown in Figures 13 and 14 are independent of λ and θ_ℓ, the curves plotted in these figures will vary only a little when different values of λ and θ_ℓ are chosen. These curves can be easily approximated taking the pertinent values of $\theta^E_{\min}$, $g(\theta^E_{\min})$ and γ_{th} from Table 3.

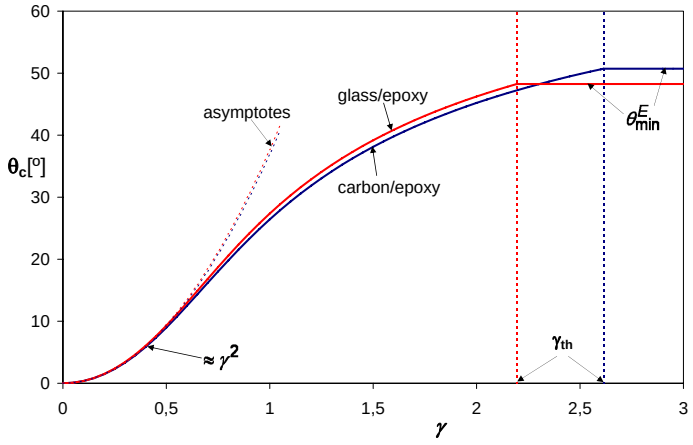

(a)

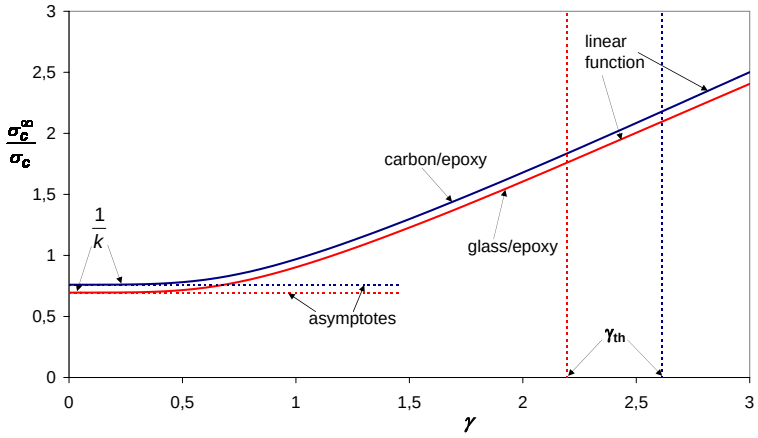

(b)

Figure 13: (a) Critical semiangle θ_c and (b) Critical remote tension as functions of the dimensionless structural parameter γ, taking $\lambda = 0.3$ and $\theta_\ell = 0.1°$.

After the abrupt crack onset of a semiangle θ_c predicted by the coupled stress and energy criterion, a further growth of the sharp interface crack can be assessed by the criterion of the classical 'infinitesimal' Interfacial Fracture Mechanics, in a similar way to that carried out, for instance, in París et al. (2007). This means that the crack of a semidebond angle θ_d is assumed to grow along the interface if

$$G(\theta_d) \geq G_c(\psi(\theta_d)). \tag{63}$$

Let θ_a ($\theta_a \geq \theta_c$) denote the arrest angle, defined as the maximum angle θ_d for which (63) holds. According to the analysis of relationships between G and G_c in Section 5.2, and in particular according to the examples shown in Figure 10, the following two post crack-onset scenarios can be expected:

a) If $\theta_c < \theta^E_{\min}$ (scenario A without the upper limit case), then $G(\theta_c) > G_c(\psi(\theta_c))$ and also $G(\theta^E_{\min}) >$

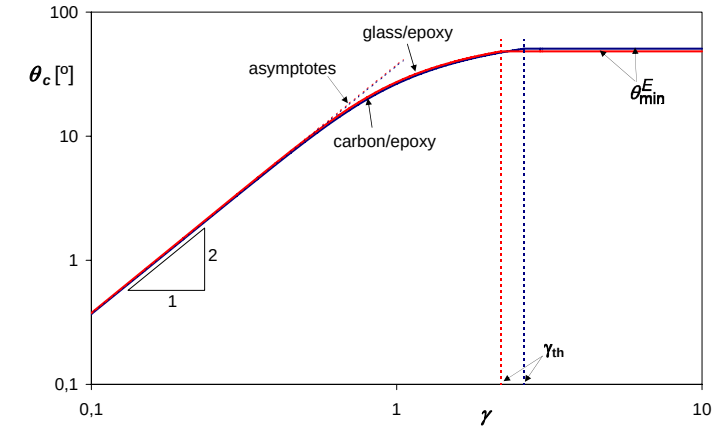

(a)

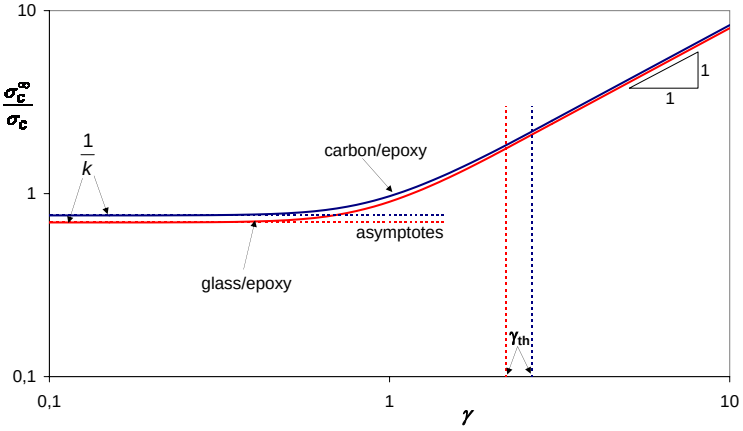

(b)

Figure 14: (a) Critical semiangle θ_c and (b) Critical remote tension as functions of the dimensionless structural parameter γ in log-log scale, taking $\lambda = 0.3$ and $\theta_\ell = 0.1°$.

$G_c(\psi(\theta^E_{\min}))$. Thus, the interface crack is expected to continue growing unstably from θ_c to $\theta_a > \theta^E_{\min}$, cf. Figure 10(a).

b) If $\theta_c = \theta^E_{\min}$ (scenario B and the upper limit of scenario A), then $G(\theta_c) = G_c(\psi(\theta_c))$ and $\mathrm{d}G(\theta_d)/\mathrm{d}\theta_d|_{\theta_d=\theta_c} < \mathrm{d}G_c(\psi(\theta_d))/\mathrm{d}\theta_d|_{\theta_d=\theta_c}$. Thus, no further unstable crack growth along the interface is expected and $\theta_a = \theta^E_{\min}$, cf. Figure 10(b).

6 Size effect

A size effect in the problem under study can be understood as a variation of the critical value of the remote tension σ_c^∞ with variations of the inclusion radius a, keeping all other problem parameters, namely the bimaterial properties (α, β, E^*) and the interface properties (σ_c, G_{1c}), constant. Thus, according to the previous analysis, and particularly in view of the dependence of the key dimensionless parameter γ defined in (52) on the inclusion radius a, some size effect governing the crack onset at the cylindrical inclusion/matrix interface can be expected. This predicted size effect appears basically due to the fact that from the four basic magnitudes appearing in the coupled stress and energy criterion, interface traction distribution (6), interface strength σ_c, ERR (16), and the interface fracture toughness (30), the only magnitude dependent on the inclusion radius a (assuming a physically reasonable range for a) is the ERR $G(\theta_d)$.

Let a bimaterial characteristic length a_0 be defined in terms of the interface properties σ_c and G_{1c} and of

the elastic bimaterial property E^* as follows[6]:

$$a_0 = \frac{G_{1c}E^*}{\sigma_c^2}, \qquad \text{thus} \qquad \gamma = \sqrt{\frac{a_0}{a}}. \tag{64}$$

Hence, $a = a_0$ is equivalent to $\gamma = 1$. Additionally, let a threshold value of a be defined as

$$a_{\text{th}} = \frac{a_0}{\gamma_{\text{th}}^2}. \tag{65}$$

For $a < a_{\text{th}}$, the interface crack onset is essentially governed by the energy criterion, and relationships (60) and (61) directly imply, in view of (43), that

$$\theta_c = \theta_{\min}^E, \qquad \text{and} \qquad \frac{\sigma_c^\infty}{\sigma_c} = \frac{\sigma_c^{\infty,E}}{\sigma_c} = \sqrt{g(\theta_{\min}^E)}\sqrt{\frac{a_0}{a}}. \tag{66}$$

Thus θ_c is constant, whereas $\sigma_c^\infty \sim \frac{1}{\sqrt{a}}$. According to the left equation in (66), the initial semilength of the interface crack, $a\theta_c$, is varying linearly with a for $a < a_{\text{th}}$.

For sufficiently large a, relationships (58) and (59) yield

$$\theta_c \cong \frac{2\cosh^2(\pi\varepsilon)}{\pi\,(1+4\varepsilon^2)}\frac{a_0}{a}, \qquad \text{and} \qquad \frac{\sigma_c^\infty}{\sigma_c} \gtrsim k^{-1}, \tag{67}$$

thus $\theta_c \sim \frac{1}{a}$, whereas σ_c^∞ is essentially governed by the stress criterion and is approaching a constant. From the left equation in (67) it follows that the initial semilength of the interface crack is approaching a constant for sufficiently large a,

$$a\theta_c \cong \frac{2\cosh^2(\pi\varepsilon)}{\pi\,(1+4\varepsilon^2)}a_0. \tag{68}$$

This result corresponds to the fact that, for a very small θ_c, the crack onset problem at the concentration point of normal tensions at the inclusion/matrix interface is locally similar to the problem of a crack situated at an infinite straight interface subjected to a remote tension $k\sigma^\infty$.

For the bimaterials defined in Table 1, Figure 15 shows θ_c, $a\theta_c$ and $\frac{\sigma_c^\infty}{\sigma_c}$ as functions of the inclusion radius a, taking $\theta_\ell = 0.1^\circ$ and $\lambda = 0.3$. Notice that $\frac{a_{\text{th}}}{a_0} = 0.21$ and 0.15 for glass/epoxy and carbon/epoxy, respectively. The corresponding plots in log-log scale are presented in Figure 16.

From the above analytic results and from Figures 15 and 16, one can conclude that, for the same bimaterial and the same quality of the interface,

- the critical crack semiangle θ_c is constant for small a, and decreases, proportionally to $\frac{1}{a}$, for increasing and large a,
- the critical crack semilength $a\theta_c$ varies linearly for small a, and approaches a constant for large a,
- the critical remote tension σ_c^∞ is increasing as $\frac{1}{\sqrt{a}}$ for decreasing and small a, and is approaching a constant for large a.

Finally, for the bimaterials defined in Table 1, values of the parameters defined in the procedure developed are shown in Table 4. These parameters have been computed assuming the inclusion radius $a = 7.5\mu$m (taken from París et al. (2007)), with $\lambda = 0.3$ and $\theta_\ell = 0.1^\circ$. As the interface strength σ_c and fracture toughness G_{1c} parameters are difficult to know precisely, roughly estimated minimum and maximum values of these parameters from the data available in Varna et al. (1997b); Zhang et al. (1997); Soden et al. (1998) are used in Table 4. In fact, σ_c values are only estimated from the bulk epoxy tensile strength values given in these references. Taking either the minimum σ_c and maximum G_{1c} or viceversa, the minimum and maximum values of each parameter presented are obtained. It can be seen that for both bimaterials $\gamma < \gamma_{\text{th}}$ (cf. Table 3), or equivalently $a > a_{\text{th}}$, thus in all the cases shown the critical values θ_c and σ_c^∞ are determined by combining both stress and energy criteria (the situation corresponding to scenario A described in Section 5.3).

[6] Analogous material characteristic lengths have previously been introduced by several authors in different contexts, e.g., the critical length for quasibrittle materials $\ell_c = \frac{EG_c}{f_t^2}$, f_t being the tensile strength, by Hillerborg et al. (1976). The length a_0 is also related to the plastic zone correction factor in a ductile material, $r_{YS} = \frac{1}{2\pi}\frac{K^2}{\sigma_{YS}^2}$, by Irwin (1960). Nevertheless, it seems that the present definition of a_0 is the first proposal of a characteristic length of this kind for interface cracks. In fact, a_0 could be considered as a generalization of the Hillerborg's critical length ℓ_c to interface cracks.

Bimaterial	σ_c [MPa]	G_{1c} [Jm^{-2}]	a_0 [μm]	a_{th} [μm]	$\frac{a}{a_0}$	γ	θ_c [°]	$\frac{\sigma_c^\infty}{\sigma_c}$
glass/epoxy	60	10	16.7	3.5	0.4	1.5	39	1.2
	90	2	1.5	0.3	5.1	0.4	7.4	0.7
carbon/epoxy	60	10	14.1	2.1	0.5	1.4	35.7	1.2
	90	2	1.3	0.2	6.0	0.4	6.1	0.8

Table 4: Estimations of the maximum and minimum values of a_0, a_{th}, a/a_0, γ, θ_c, σ_c^∞/σ_c for the examples of isotropic bimaterials.

7 Concluding remarks

1) A theoretical model has been developed for the prediction of the crack onset at the interface between a stiff circular cylindrical inclusion and a compliant unbounded matrix subjected to a remote uniaxial transverse tension. This model is based on a coupled pointwise stress criterion and an incremental energy criterion, an approach recently introduced by Leguillon (2002). The inclusion and matrix materials are assumed to be homogeneous isotropic linearly elastic, bonded along a strong and brittle interface. The interface is characterized by two failure parameters: the tensile strength σ_c and the fracture toughness curve $G_c(\psi)$, ψ being the fracture mode mixity angle. At onset, an abrupt crack formation of a finite extension is assumed to occur around the tensile traction concentration point at the interface. The present coupled stress and energy criterion predicts the critical value of the remote load σ_c^∞ and the initial crack angle θ_c at onset.

2) The predicted values of σ_c^∞ (normalized by σ_c) and θ_c are determined as functions of the Dundurs bimaterial parameters α and β and of a new dimensionless microstructural parameter γ (52). The parameter γ has shown to be suitable for characterization of the present crack onset problem. It is closely related to a characteristic length parameter a_0 (64), defined in terms of the interface tensile strength σ_c, the interface fracture toughness G_{1c} associated to the fracture Mode I, and the harmonic mean E^* of the effective elastic moduli of the inclusion and matrix. The parameter γ can be defined as the square root of the ratio of a_0 to the inclusion radius a. Therefore, a size effect, i.e. variations of predicted values of σ_c^∞ and θ_c with a keeping all other problem parameters constant, is inherent to the predictions obtained. Basically, this size effect is associated to the fact that the crack Energy Release Rate (ERR) decreases as a decreases for the same remote load applied, whereas the effect of a variation (in a physically reasonable length range) on the interface fracture toughness is negligible. Notice also that the stress criterion alone is not able to predict any size effect, as the interfacial stress distribution is independent of a, considering that the effect of a variation on the interface strength is negligible.

3) The asymptotic behaviour of the predicted values of σ_c^∞ and θ_c for small and large values of a can be characterized in simple terms as follows. For small values of a, the crack onset of a constant angle θ_c (independent of a) is expected to occur, while the critical remote tension σ_c^∞ is increasing as $\sim \frac{1}{\sqrt{a}}$ with decreasing a. For large values of a, the semilength of the crack $a\theta_c$ at onset and the critical remote tension σ_c^∞ are approximately constant. The former size effect feature seems to be in accordance with the experimental evidence that, in general, the tensile strength of composites increases as the inclusion size decreases. Nevertheless, it might be possible that although for very small values of a the interface debond will not occur, rupture of the matrix near the inclusion could instead become the preferred mode of failure.

4) With reference to the size effect studied, considering different inclusion radii a, one could argue that the application of a fixed material-based reference length ℓ_m to define the fracture mode mixity angle ψ would be a more consistent choice than the geometry-based reference length $\ell_g = \theta_\ell a$ (θ_ℓ being a small fixed reference angle) used in the present work. The reference length ℓ_g is adopted in the present work for the sake of simplicity and the universality of the analysis performed, being perfectly consistent for the study carried out in Section 5. Nevertheless, to check the influence of this choice on the size effect studied in Section 6, additional calculations have been performed for a small and physically reasonable $\ell_m = 0.1° \times 7.5\mu\text{m} = 0.013\mu\text{m}$. The four limit cases of the characteristic length parameter a_0 presented in Table 4 have been analysed. Only slight deviations have been observed from the plots shown in Figures 15 and 16 for glass/epoxy, these deviations being even smaller for carbon/epoxy. In fact, in large parts of some plots the differences are hardly visible. Considering a physically reasonable range $0.1 \leq a/a_0 \leq 10$, the maximum relative differences between the values of the three quantities presented in these plots (θ_c, $\theta_c a/a_0$ and σ_c^∞/σ_c) obtained using ℓ_m and ℓ_g have been less than 9% for glass/epoxy and less than 3% for carbon/epoxy. In particular, with reference to the predicted behaviour $\sigma_c^\infty \sim \frac{1}{\sqrt{a}}$ for small values of a, the least squares fitting of power law in the range $0.1 \leq a/a_0 \leq a_{\text{th}}/a_0$ gives the exponents whose relative differences from -0.5 are less than 6% and close to 1%, respectively, for the

couples of large and small values of a_0 in Table 4. Thus, the choice of a small and physically reasonable ℓ_m affects only weakly the size effect predicted by using ℓ_g. It can be expected that the size effect characteristics extracted from the behaviour of θ_c, $\theta_c a$ and σ_c^∞ in Figures 15 and 16, obtained using ℓ_g, represent a good universal approximation of the behaviour of these quantities when obtained using other physically reasonable choices of ℓ_m.

5) It should be mentioned that, although the present work has mainly focused on the interface crack onset, a simple analysis of the post crack-onset behaviour has also been introduced. The key parameter of this analysis is the angle $\theta^E_{\min}$ (38), the upper bound for θ_c. If $\theta_c < \theta^E_{\min}$ then a further unstable crack growth along the inclusion/matrix interface can be expected up to an arrest angle greater than $\theta^E_{\min}$. However, if $\theta_c = \theta^E_{\min}$, no further crack growth along the interface is expected for the remote load value considered. A more detailed and realistic analysis of this post crack-onset behaviour can be carried out by the suitable analytical and numerical tools presented in París et al. (2007). In fact, according to the results of the numerical study presented therein, it can be expected that the interface crack will grow unstably up to semidebonding angles of values $60° - 70°$, where it will either stop or continue growing along the interface or kink towards the matrix, then continuing its unstable growth as a matrix crack in the direction perpendicular to the load. If the latter scenario represents reasonably the real progression of damage in a unidirectional ply under transverse tension, assuming the coalescence of the matrix cracks initiated at the fibre/matrix interfaces, then the critical load for the interface crack onset predicted in the present work could be quite directly related to the critical transverse tension for the whole ply.

6) It is expected that the present work can contribute to clarifying which relations of the bimaterial and fibre/matrix interface properties play an important role in the resulting transverse tensile strength of a unidirectional ply. These relations can be very useful in the fibre/matrix interface characterization. In particular, knowledge of the value of the parameter γ (or equivalently of the characteristic length parameter a_0), governing the interface crack onset, seems to be fundamental in this sense. Thus, it could be very useful to develop some specific experiments, for example, using single fibre specimens, to determine the value of γ for a particular fibre/matrix system.

7) The present formulation of the coupled stress and energy criterion can be easily modified by incorporating the average instead of the pointwise tensile stress criterion employed here, as suggested by Cornetti et al. (2006) and Carpinteri et al. (2008). It has been checked that visible differences between the predictions obtained by the coupled criteria, using one of these two tensile stress criteria, appear only in the transition regime between the two asymptotic regimes, corresponding to small and large inclusion radii a. In fact, there is no difference between the application of these stress criteria once sufficiently small inclusion radii a are considered, as for these a the debond onset is governed by the energy criterion only. Also, the differences between the predictions obtained using these stress criteria are hardly visible for large a, as these predictions are governed by the same asymptotes. The main difference between the application of these stress criteria is the threshold value a_{th}, which is several times greater for the average than for the pointwise tensile stress criterion (e.g. about 3.3 times for glass/epoxy and 4.1 times for carbon/epoxy, taking $\lambda = 0.3$ and a small reference angle $\theta_\ell = 0.1°$).

An application of the Mohr-Coulomb pointwise stress criterion in the coupled stress and energy criterion could also be of interest, considering large shear tractions acting along the inclusion/matrix interface for the values of the polar angle θ close to 45°. As the Mohr-Coulomb criterion can predict the position of the debond initiation at an angle θ different from 0°, such an application would be more challenging, requiring to analyse asymmetric configurations of the load and an asymmetrically growing debond.

Experimental evidence would be necessary to determine which of these criteria is the best suited to the present problem.

8) The present approach can also be extended to the cylindrical inclusion/matrix configuration subjected to other kinds of remote transverse loads, like compression, Correa et al. (2008a,b), or biaxial loads, París et al. (2003), to obtain pertinent predictions of the critical load initiating an interface debond. Such studies could further contribute to a better understanding of the FRC strength under transverse loads.

Acknowledgement

The author thanks Prof. Federico París for his motivation and continuous support of this work. Comments by Prof. Federico París and Dr. Enrique Graciani have substantially improved the final version of the manuscript. Stimulating discussions with Dr. Elena Correa and use of her Mathematica code of the Toya's solution are also gratefully acknowledged. This work was supported by the Spanish Ministry of Education, Culture and Sport through Project TRA2005-06764, and by the Junta de Andalucía, through the Project of Excellence TEP1207. Part of the present work was performed during a research stay at the Oak Ridge National Laboratory (ORNL)

in 2008. The support of this stay by Dr. Len Gray (ORNL) and by the Junta de Andalucía (Estancia de excelencia) is also gratefully acknowledged.

A Proof of inequality $\frac{\mathbf{d}G(\theta_d)}{\mathbf{d}\theta_d} < \frac{\mathbf{d}G_c(\psi(\theta_d))}{\mathbf{d}\theta_d}$ for $\theta_d = \theta_c^E = \theta_{\mathbf{min}}^E$

Let $\theta_c^E = \theta_{\min}^E$. By the definition of θ_c^E, as the minimum angle $\Delta\theta > 0$ for which equality holds in (35),

$$\int_0^{\Delta\theta} G(\theta_d)\mathrm{d}\theta_d < \int_0^{\Delta\theta} G_c(\psi(\theta_d))\mathrm{d}\theta_d, \quad \text{for} \quad 0 < \Delta\theta < \theta_{\min}^E, \tag{69}$$

$$\int_0^{\theta_{\min}^E} G(\theta_d)\mathrm{d}\theta_d = \int_0^{\theta_{\min}^E} G_c(\psi(\theta_d))\mathrm{d}\theta_d. \tag{70}$$

Hence, by subtracting (70) from (69),

$$\int_{\Delta\theta}^{\theta_{\min}^E} G(\theta_d)\mathrm{d}\theta_d > \int_{\Delta\theta}^{\theta_{\min}^E} G_c(\psi(\theta_d))\mathrm{d}\theta_d, \quad \text{for} \quad 0 < \Delta\theta < \theta_{\min}^E. \tag{71}$$

According to definitions (16) and (30), see also Figures 6 and 8, the functions $-G(\theta_d)$ and $G_c(\psi(\theta_d))$ are strictly convex in the range of angles of interest for the present study, say $\theta_d \leq 80°$. Then, the left part of the Hermite-Hadamard inequality for strictly convex functions applied to the members of the inequality (71) yields the following inequality chain for $0 < \Delta\theta < \theta_{\min}^E$:

$$G\left(\frac{\Delta\theta + \theta_{\min}^E}{2}\right) > \frac{1}{\theta_{\min}^E - \Delta\theta}\int_{\Delta\theta}^{\theta_{\min}^E} G(\theta_d)\mathrm{d}\theta_d > \frac{1}{\theta_{\min}^E - \Delta\theta}\int_{\Delta\theta}^{\theta_{\min}^E} G_c(\psi(\theta_d))\mathrm{d}\theta_d > G_c\left(\psi\left(\frac{\Delta\theta + \theta_{\min}^E}{2}\right)\right). \tag{72}$$

Considering the first and the last terms in (72) leads directly to the following general inequality in the case $\theta_c^E = \theta_{\min}^E$:

$$G(\theta_d) > G_c(\psi((\theta_d)), \quad \text{for} \quad \frac{\theta_{\min}^E}{2} < \theta_d < \theta_{\min}^E. \tag{73}$$

Applying a basic property of differentiable strictly convex functions to the members of (73) gives

$$G\left(\theta_{\min}^E\right) + \left.\frac{\mathrm{d}G}{\mathrm{d}\theta_d}\right|_{\theta_d=\theta_{\min}^E}\left(\theta_d - \theta_{\min}^E\right) > G(\theta_d) > G_c(\psi(\theta_d)) > G_c\left(\psi\left(\theta_{\min}^E\right)\right) + \left.\frac{\mathrm{d}G_c}{\mathrm{d}\theta_d}\right|_{\theta_d=\theta_{\min}^E}\left(\theta_d - \theta_{\min}^E\right), \tag{74}$$

for $\frac{\theta_{\min}^E}{2} < \theta_d < \theta_{\min}^E$. Then, in view of the equality in (40),

$$\left.\frac{\mathrm{d}G}{\mathrm{d}\theta_d}\right|_{\theta_d=\theta_{\min}^E} < \left.\frac{\mathrm{d}G_c}{\mathrm{d}\theta_d}\right|_{\theta_d=\theta_{\min}^E}. \tag{75}$$

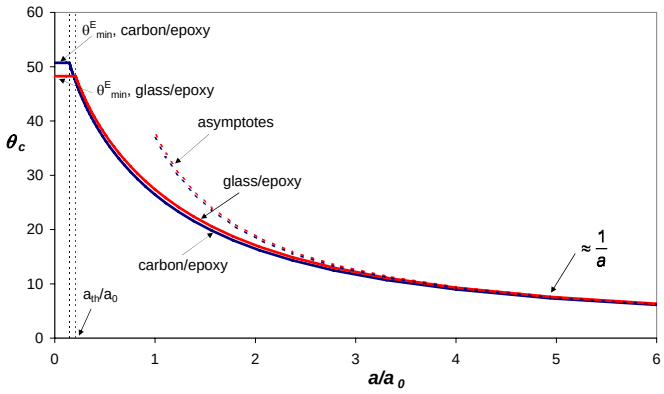

(a)

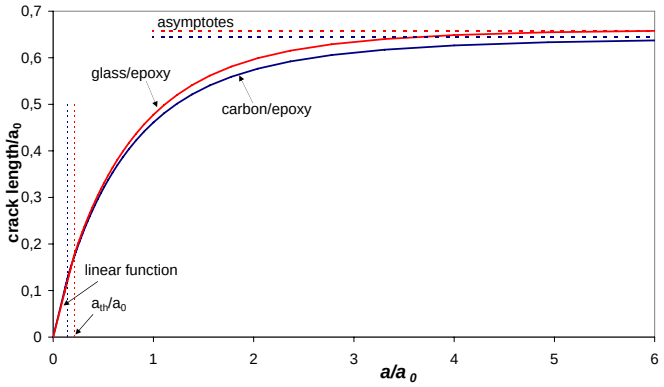

(b)

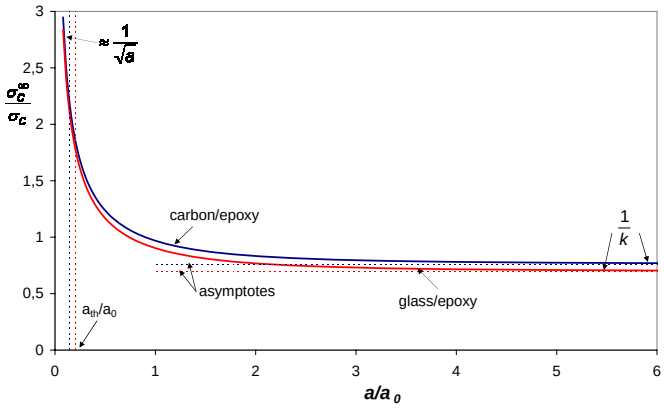

(c)

Figure 15: (a) Critical semiangle θ_c, (b) Critical semilength of the crack $a\theta_c$ and (c) Critical remote tension σ_c^∞ as functions of the inclusion radius a, taking $\lambda = 0.3$ and $\theta_\ell = 0.1°$.

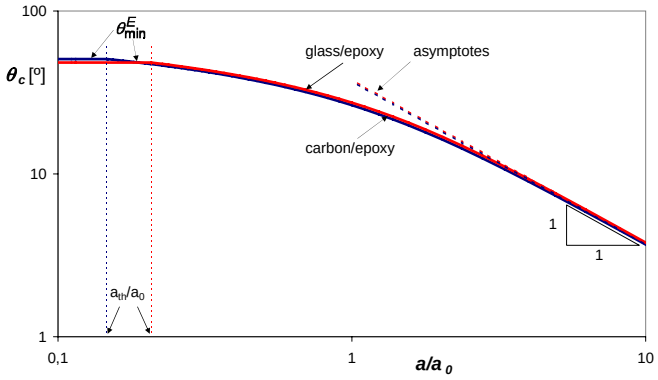

(a)

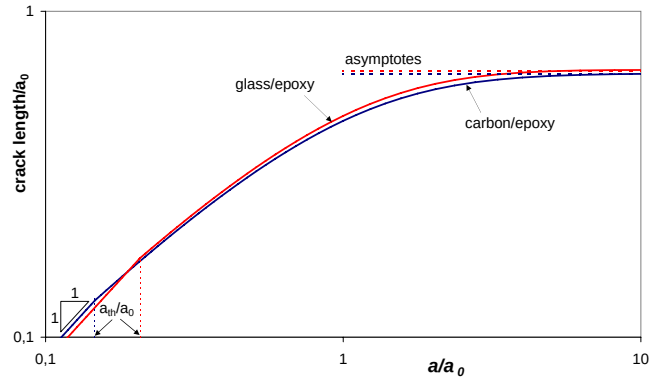

(b)

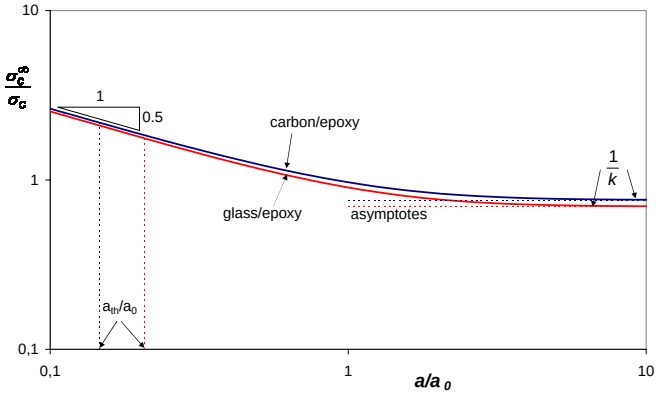

(c)

Figure 16: (a) Critical semiangle θ_c, (b) Critical semilength of the crack $a\theta_c$ and (c) Critical remote tension σ_c^∞ as functions of the inclusion radius a in log-log scale, taking $\lambda = 0.3$ and $\theta_\ell = 0.1°$.

References

Agrawal, A., Karlsson, A.M., 2007. On the reference length and mode mixity for a bimaterial interface. Journal of Engineering Materials and Technology 129, 580-587.

Banks-Sills, L., Ashkenazi, D., 2000. A note on fracture criteria for interface fracture. International Journal of Fracture, 103, 177–188.

Barenblatt, G.I., 1993. Some general aspects of fracture mechanics. In: Modelling of Defects and Fracture Mechanics, G. Herrmann (Ed.), Springer-Verlag, Wien, New York, 29–59.

Carpinteri, A., 1981. Size effect in fracture toughness testing: A dimensional analysis approach, in Analytical and Experimental Fracture Mechanics (Proc. of an Int. Conf., Roma, Italy, 1980), G.C. Sih, M. Mirabile (Eds.), Sijthoff & Noordhoff, Alphen aan den Rijn, 785–797.

Carpinteri, A., 1982. Notch sensitivity in fracture testing of aggregative materials. Engineering Fracture Mechanics, 16, 467–481.

Carpinteri, A., Cornetti, P., Pugno, N., Sapora, A., Taylor, D., 2008. A finite fracture mechanics approach to structures with sharp V-notches. Engineering Fracture Mechanics, 75, 1736–1752.

Chao, R., Laws, N., 1997. The fiber-matrix interface crack. Journal of Applied Mechanics 64, 992–999.

Cho, J., Joshi, M.S., Sun, C.T., 2006. Effect of inclusion size on mechanical properties of polymeric composites with micro and nano particles. Composites Science and Technology 66, 1941–1952.

Comninou, M., 1977. The interface crack. Journal of Applied Mechanics 44, 631–636.

Cornetti, P., Pugno, N., Carpinteri, A., Taylor, D., 2006. Finite fracture mechanics: A coupled stress and energy failure criterion. Engineering Fracture Mechanics 73, 2021–2033.

Correa, E., Mantič, V., París, F., 2008a. Numerical characterisation of the fibre-matrix interface crack growth in composites under transverse compression. Engineering Fracture Mechanics 75, 4085-4103.

Correa, E., Mantič, V., París, F., 2008b. A micromechanical view of inter-fibre failure of composite materials under compression transverse to the fibres. Composites Science and Technology 68, 2010-2021.

Dundurs, J., 1969. Discussion of a paper by D.B. Bogy. Journal of Applied Mechanics 36, 650–652.

England, A.H., 1966. An arc crack around a circular elastic inclusion. Journal of Applied Mechanics 33, 637–640.

Fisher, J.R., Gurland, J., 1981. Void nucleation in spheroidized carbon steels - 2. Model. Metal Science 15, 193–202.

Gerberich, W., Yang, W. (Eds.), 2003. Interfacial and Nanoscale Failure (Vol. 8), In: Comprehensive Structural Integrity, Editors-in-Chief I. Milne, R.O. Ritchie and B. Karihaloo, Elsevier Pergamon, Amsterdam.

Goodier, J.N., 1933. Concentration of stress around spherical and cylindrical inclusions and flaws. Journal of Applied Mechanics 55, 39–44.

Graciani, E., Mantič, V., París, F., 2007. On the estimation of the first interpenetration point in the open model of interface cracks. International Journal of Fracture 143, 287–290.

Hardiman, N.J., 1954. Elliptic Elastic Inclusion in an Infinite Elastic Plate. The Quarterly Journal of Mechanics and Applied Mathematics 7, 226–230.

Hillerborg, A., Modéer, M., Petersson, P.E., 1976. Analysis of crack formation and crack growth in concrete by means of fracture mechanics and finite elements. Cement and Concrete Research, 6, 773–782.

Hills, D.A., Barber, J.R., 1993. Interface cracks. International Journal of Mechanical Sciences 35, 27–37.

Hills, D.A., Kelly, P.A., Dai, D.N., Korsunsky, A.M., 1996. Solutions of Crack Problems. The Distributed Dislocation Technique, Kluwer Academic Publishers, Dordrecht.

Honein, T., Herrmann, G., 1990. On bonded inclusions with circular or straight boundaries in plane elastostatics. Journal of Applied Mechanics 57, 850–856

Hutchinson, J.W., Suo, Z., 1992. Mixed mode cracking in layered materials. Advances in Applied Mechanics 29, 63–191.

Irwin, G.R., 1960. Plastic zone near a crack and fracture toughness, In: Mechanical and Metallurgical Behaviour of Sheet Materials, Proceedings of the Seventh Sagamore Ordnance Materials Research Conference, Vol. IV. Syracuse University Press, pp. 63–78.

Leidner, J., Woodhams, R.T., 1974. The strength of polymeric composites containing spherical fillers. Journal of Applied Polymer Science 18, 1639–1654.

Leguillon, D., 2002. Strength or toughness? A criterion for crack onset at a notch. European Journal of Mechanics A/Solids 21, 61–72.

Leguillon, D., Siruguet, K., 2002. Finite fracture mechanics - application to the onset of a crack at a bimaterial corner. In: Karihaloo, B.L. (ed.), IUTAM Symposium on Analytical and Computational Fracture Mechanics of Non-Homogenous Materials. Kluwer Academic Publishers, pp. 11–18.

Leguillon, D., Quesada, D., Putot, C., Martin, E., 2007. Prediction of crack initiation at blunt notches and cavities - size effect. Engineering Fracture Mechanics 74, 2420–2436.

Mantič, V., 2008. Discussion of a paper by A. Agrawal, A. and A.M. Karlsson. Journal of Engineering Materials and Technology 130, 045501-1–2, DOI:10.1115/1.2975231.

Mantič, V., París, F., 2004. Relation between SIF and ERR based measures of fracture mode mixity in interface cracks. International Journal of Fracture 130, 557–569.

Mantič, V., Blázquez, A., Correa, E., París, F., 2006. Analysis of interface cracks with contact in composites by 2D BEM. In: Guagliano, M., Aliabadi, M.H. (Eds.), Fracture and Damage of Composites (Chapter 8). Wessex Institute of Technology Press, pp. 189–248.

Murakami, Y., 1988. Stress Intensity Factor Handbook. Oxford, Pergamon Press.

París, F., del Caño J.C., Varna J., 1996. The fibre-matrix interface crack - A numerical analysis using boundary elements. International Journal of Fracture 82, 11–29.

París, F., Correa E. and Cañas, J., 2003. Micromechanical view of failure of the matrix in fibrous composite materials. Composites Science and Technology, 63, 1041–1052.

París, F., Correa, E., Mantič, V., 2007. Kinking of transverse interface cracks between fibre and matrix. Journal of Applied Mechanics 74, 703–716.

Prasad, P.B.N., Simha, K.R.Y., 2003. Interface crack around circular inclusion: SIF, kinking, debonding energetics. Engineering Fracture Mechanics 70, 285–307.

Rice, J.R., 1988. Elastic fracture mechanics concepts for interfacial cracks. Journal of Applied Mechanics 55, 98–103.

Soden, P.D., Hinton, M.J., Kaddour. A.S., 1998. Lamina properties, lay-up configurations and loading conditions for a range of fibre-reinforced composite laminates. Composites Science and Technoloy, 58, 1011–1022.

Taylor, D., Cornetti, P., Pugno, N., 2005. The fracture mechanics of finite crack extension. Engineering Fracture Mechanics 72, 1021–1038.

Toya, M., 1974. A crack along the interface of a circular inclusion embedded in an infinite solid. Journal of the Mechanics and Physics of Physics Solids 22, 325–348.

Tszeng T. C., 1993. A model of void nucleation from ellipsoidal inclusions in ductile fracture. Scripta Metallurgica et Materialia 28, 1065–1070.

Varna, J., París, F., del Caño, J.C., 1997a. The effect of crack-face contact on fiber/matrix debonding in transverse tensile loading. Composites Science and Technology 57, 523–532.

Varna, J., Berglund, L. A. and Ericson, M. L., Transverse single fibre test for interfacial debonding in composites 2: Modelling, Composites Part A 28 , 317–326.

Williams, M.L., 1959. The stress around a fault of crack in dissimilar media. Bull. Seismol. Soc. Am. 49, 199–204.

Zhang H., Ericson M.L., Varna J., Berglund L.A., 1997. Transverse single-fibre test for interfacial debonding in composites: 1. Experimental observations. Composites Part A 28, 309–315.